Universidade do Porto

FEUP Faculdade de Engenharia

Ângela Marisa Pereira Carvalho

Development of nanostructured and bioactive surfaces onto ceramic substrates

Porto, 2011

Ângela Marisa Pereira Carvalho

Development of nanostructured and bioactive surfaces onto ceramic substrates

Work presented to the Faculty of Engineering of the University of Porto as part of the requirements for the Degree of Master in Biomedical Engineering under the supervision of Professor Fernando Jorge Monteiro from Faculty of Engineering of the University of Porto, and having Dr. Alejandro Pelaez-Vargas from INEB, as advisor

ABSTRACT

Recent developments in biomaterials are associated to changes in concepts and applications. Some biomaterials that were used in the past for a certain application may not be used nowadays due to improvements or substitutions for a better material. The constant search for a biomaterial that might last for the whole patient's life is still a challenge in almost every clinical application.

In oral surgery, teeth are likely candidates for replacement by artificial components such as orthodontic implants. Overall, this approach is highly successful; however, restorative surgery involving implants generally have a finite lifespan and may require replacement at a future time. The main material used as implant in dentistry is titanium. This has shown good properties to be applied as a dental implant, as the fact that it promotes osseointegration; it is biocompatible and has excellent mechanical properties. However, titanium is also associated to some disadvantages. This material is associated with allergic reactions in some persons, gingival tarnishing and peri-implantitis, an infection in the support tissues around the implant provoked by bacterial colonization and reduced tissue attachment that causes bone loss.

In this work, a new approach to modify ceramic (zirconia) dental implants surface is presented. The main goal is to use a bioactive and micropatterned silica coating to increase osteointegration and cell modulation for guided tissue regeneration and to diminish the bacterial adhesion and proliferation at the implant-tissue interface, eliminating also gingival tarnishing problems.

Silica was produced by the sol-gel method to obtain a more homogeneous and purer glass. Soft-lithography was used to generate Polydimethylsiloxane (PDMS) negative molds with line-shaped features. Nanohydroxyapatite was added to the silica in two different percentages: 1% and 5%.

The three types of silica coatings were produced by stamping a small amount of the solutions onto a glass substrate with the PDMS mold and a flat silica control was produced by spin-coating. Thin films surfaces were characterized in terms of composition, hydrophobicity and relative elemental percentages.

In vitro biological studies in terms of bacterial adhesion and proliferation and cell citocompatibility, viability and oriented proliferation were performed. Human pulp derived mesenchymal stem cells were cultured over the various types of materials and their differentiation into osteoblast was also assessed. Streptococcus mutans initial adhesion and proliferation to the various surfaces was also evaluated.

According to the results, the patterned surfaces were biocompatible and affected cell orientation that presented an elongated morphology along the micropattern features at all time points. Mesenchymal stem cells differentiation into osteoblasts was also achieved as confirmed by ALP activity, alizarin red staining, mineralization process detection and RT-PCR results. Overall, the cultured cells on the different thin films showed similar results in all the evaluated parameters.

Regarding the bacterial adhesion, *S.mutans* was able to attach and proliferate to all the thin films and EPS production was observed after 90 minutes of adhesion time and 72h of biofilm formation. It was observed that the inclusion of the patterns and of nanoHA particles significantly increased bacterial adhesion.

RESUMO

O desenvolvimento de biomateriais está relacionado com mudanças em conceitos e aplicações. Alguns biomateriais que foram usados no passado para uma certa aplicação podem já não ser utilizados actualmente devido a optimizações ou substituições por um material melhor. A constante procura por um biomaterial que possa durar toda a vida de um paciente ainda constitui um desafio em quase todas as aplicações clínicas.

Em cirurgia oral, os dentes são candidatos óbvios à substituição por componentes artificiais tais como implantes dentários. Globalmente, esta abordagem é bem sucedida, no entanto, as cirurgias restaurativas que envolvem implantes têm em conta que os implantes possuem um tempo de vida finito e a sua substituição pode ser necessária no futuro.

O principal material usado como implante dentário é o Titânio. Este material tem demonstrado boas propriedades para ser utilizado como implante nesta aplicação, pelo facto de promover a osteointegração, ser biocompatível e ter excelentes propriedades mecânicas. No entanto, o titânio também demonstra algumas desvantagens. Este material tem sido associado a reacções alérgicas em alguns pacientes, coloração das gengivas e peri-implantite, uma infecção nos tecidos que circundam o implante, provocada por colonização bacteriana e baixa adesão tecidular, o que induz perda óssea.

Neste trabalho, é apresentada uma nova abordagem para modificar a superfície de implantes dentários cerâmicos (Zircónia). O principal objectivo é recorrer ao uso de um revestimento bioactivo e microtexturado de sílica para aumentar a osteointegração e modular a proliferação celular, criando regeneração guiada do tecido e diminuindo a adesão e proliferação bacteriana no interface implante-tecido, eliminando também os problemas associados à coloração das gengivas.

A sílica foi produzida pelo método de *Sol-gel* de forma a gerar um vidro mais puro e homogéneo. A técnica de *Litografia Suave* foi utilizada para produzir moldes negativos de polidimetilsiloxano (PDMS) com um padrão de linhas. Partículas de nanohidroxiapatite foram adicionadas à sílica em duas percentagens diferentes: 1% e 5%.

Os três tipos de revestimentos de sílica foram obtidos recorrendo à estampagem, com os moldes de PDMS, de uma pequena quantidade das soluções num substrato de vidro, comparando com uma superfície controlo de sílica lisa que foi preparada por

spin-coating. A superfície dos diferentes revestimentos foi caracterizada em termos de composição, hidrofobicidade e quantidade relativa dos vários elementos.
Os revestimentos foram avaliados em estudos biológicos *in vitro* no que diz respeito a adesão e proliferação bacteriana e citocompatibilidade, viabilidade e proliferação orientada das células. Células estaminais mesenquimais derivadas de polpa humana foram cultivadas nos vários materiais e a sua diferenciação em osteoblastos foi avaliada. A adesão inicial e proliferação de Estreptococos mutans nas várias superfícies foram também estudadas.

Os resultados demonstram que as superfícies padronizadas eram biocompativeis e influenciavam a orientação celular, que apresentava uma morfologia alongada relacionada com a orientação dos micropadrões, para todos os tempos de cultura. Foi também conseguida a diferenciação das células estaminais mesenquimais em osteoblastos, confirmada através dos resultados da actividade da ALP, coloração com alizarina vermelha, detecção de mineralização e RT-PCR. Globalmente, as células cultivadas nos vários materiais apresentaram resultados semelhantes em todos os parâmetros avaliados.
No que diz respeito à adesão bacteriana, *estreptococos mutans* pode aderir e proliferar em todos os revestimentos e a produção de substâncias poliméricas extracelulares foi observada após os 90 minutos de adesão e as 72 horas de formação de biofilme. Foi também observado que quer a existências dos padrões quer a adição das nanopartículas de hidroxiapatite aumentavam significativamente a adesão bacteriana.

Acknowledgments

First of all, I would like to thank my supervisor, Professor Fernando Monteiro, for all the help, support, counseling and availability and for giving me the opportunity of working in such an interesting project.

I would also like to thank my advisor, Alejandro Pelaez-Vargas, for all the help, opportunities and patience and for giving me the freedom to test all my ideas.

An acknowledgment to Prof. Maria Pia Ferraz and Prof. Maria Helena Fernandes for the support, transmitted knowledge and for helping me every time I needed.

To all my lab partners and friends, I thank for the companionship, the good lab environment and for everything they taught me. A special thanks to Liliana Grenho and Marta Laranjeira for helping me in specific tasks of my work.

I would like to thank Mónica Garcia, Ricardo Vidal, Ricardo Silva, Daniela Silva and Liliana Alves, the technicians from FMDUP, INEB, CEBIMED and CEMUP for all the support and the help with all the equipments.

Finally, I would like to thank my family, my friends and Leonardo for the unconditional support and for trying to understand exactly what I was doing because their contribution was determinant for the success of this work.

Summary

Illustrations Summary

Tables Summary

Abbreviations

ALP – Alkaline Phosphatase

BHI – Brain Heart Infusion

CFU – Colony Forming Unit

CLSM – Confocal Laser Scanning Microcopy

DPSC – Dental Pulp Stem Cells

EDS – Energy Dispersive X-ray Spectroscopy

EPS – Extracellular Polymeric Substances

GAPDH – Glyceraldehyde- 3-phosphate Dehydrogenase

HA – Hydroxyapatite

HCA – Hydroxycarbonate apatite layer

MSC – Mesenchymal Stem cells

MTES – Methyltriethoxisilane

NanoHA – Nanophased Hydroxyapatite

PBS – Phosphate buffered saline solution

PDMS – Polydimethylsiloxane

RT-PCR – Reverse transcriptase polymerase chain reaction

SEM – Scanning Electron Microscopy

TCP – Tissue culture poliestirene

TEOS – Tetraethylorthosilicate

TSB – Tryptic soy broth

XPS – X-Ray photoelectron spectroscopy

I. Literature Review

1. Zirconia

1.1. Source and manufacturing Zirconia

Zirconium was discovered by the German chemist Martin H. Klaproth in 1789. Pure zirconia can be obtained from chemical conversion of zircon (ZrSiO), which is an abundant mineral deposit [1, 2].

Zircon is first chlorinated to form $ZrCl_4$ in a fluidized bed reactor in the presence of petroleum coke. A second chlorination is required for high-quality zirconium. Zirconium is precipitated with either hydroxides or sulfates, and then calcinated to its oxide [2]. Zirconia (ZrO_2) has been widely used in orthopedic and dental applications [3].

1.2. Phase Structure

There are three low-pressure phases of zirconia: the monoclinic, tetragonal, and cubic, which are stable at increasingly higher temperatures. Zirconia undergoes an allotropic phase transition from monoclinic to tetragonal at 1000~1200ºC, and from tetragonal to cubic at 2370ºC, as it is shown in figure 1.1. [3]

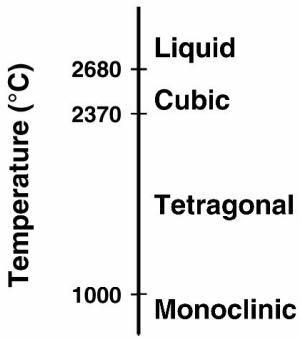

Figure 1. 1 – Temperatures in the three phases of Zirconia [4].

The phase transition from cubic to monoclinic and tetragonal is diffusionless and takes place simultaneously with a volume expansion of about 7%. The phase transition from tetragonal to monoclinic occurs upon cooling the material and is associated with a volume expansion of 3-5%, which is sufficient to exceed the material strength and results on its fracture. However, the addition of stabilizers allows maintaining the cubic

and tetragonal phases at room temperature [3-6]. In the following figure (Fig.1.2) are shown the three types of phase structure.

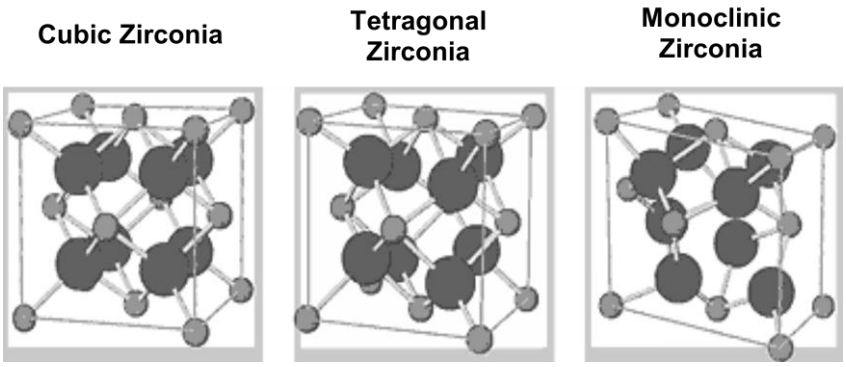

Figure 1.2 - Structure of the three phases of Zirconia [5].

1.3. Stabilization

In order to use tetragonal or cubic zirconia, these are doped with oxides such as Yttria (Y_2O_3), Magnesia (MgO), Calcium oxide (CaO), Ceria (CeO_2), that stabilize the high-temperature phases at room temperature. This procedure affects both the mechanical and electrical properties. Doping of zirconia results in stabilization of the tetragonal phase at lower dopant concentrations (for mechanical toughness) or the cubic phase at higher dopant concentrations (for high ionic conductivity) at room temperature [3, 5].

1.4. Low Temperature Degradation and Transformation Toughening

Zirconia ceramics can spontaneously revert the tetragonal phase into monoclinic phase, producing stresses, surface microcracking and lost of structural integrity in a phenomenon known as hydrothermal degradation or low temperature degradation (LTD). The stability of the tetragonal structure can be controlled by three factors: the grain size, the constraint from a surrounding matrix, and the amount of dopant additions. Transformation toughening is a mechanism that can be used to improve the toughness of zirconia by controlling the transformation process in the stress field ahead of the crack tip [7, 8]. What happens during the transformation toughening is that the volume expansion associated with the transformation from the tetragonal to monoclinic phase acts on the crack in such a way as to reduce its potential to propagate (Fig. 1.3) [4, 8].

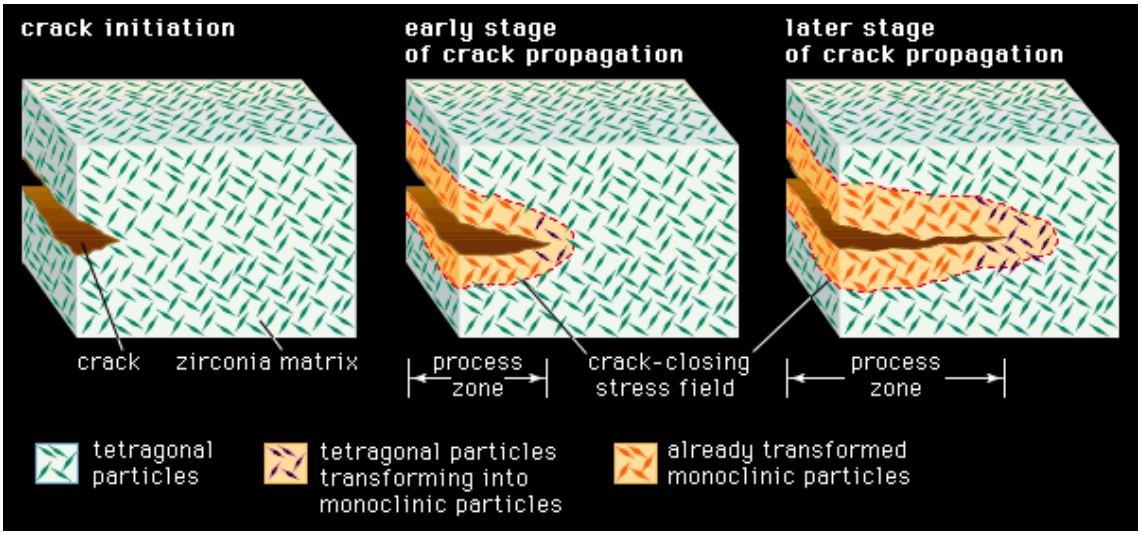

Figure 1. 3 - Resistance to cracking in transformation-toughened zirconia. In a ceramic composed of tetragonal zirconia dispersed in a zirconia matrix, the stress field advancing ahead of a propagating crack transforms the small tetragonal particles to larger monoclinic particles. The larger particles exert a crack-closing force in the process zone behind the crack tip, effectively resisting propagation of the crack [9].

1.5. Processing zirconia

The correct processing of zirconia affects the overall properties and the behavior of this ceramic, being a really important step.

A problem existing with ceramics, zirconia included, is that they exhibit high melting points, so they cannot be easily heated to their melting temperatures to be processed, as it happens with most metals and polymers. Therefore, one alternative route to this problem is the processing of powders to form the ceramic. This process involves the packing together of fine powders, their consolidation and heating to form bonds [8, 10].

The compacting of the zirconia powders will allow obtaining a dense compact material with reduced grain size, to optimize the ceramic mechanical properties [5, 10, 11]. Finally, the compact ceramic is sintered. The conventional sintering in ceramics uses high temperatures and it can be divided in three stages, shown in figure I.5. In the first stage, the powder is already compacted and the particles are in contact with each other but they are not physically bonded (Fig. 1.4 a) [8, 11].

In the second stage the compacted powder is heated to a temperature that is usually about 2/3 of its melting point. At this stage ‘necks’ begin to form between the particles, binding them together (Fig. 1.4 b). Finally, the small contact areas between particles expand, and at the same time the density of the compact increases and the total void volume decreases. In the third stage, individual particles can no longer be seen because they are fully bond together leaving residual porosity in the form of closed-off

pores that have sufficiently small diameter so as not to have a detrimental effect on the mechanical properties of the final material (Fig. 1.4 c).

The powder particle size will control the final pore size and distribution: the smaller the particle size the smaller the pores and the better the mechanical properties will be [4, 5, 8].

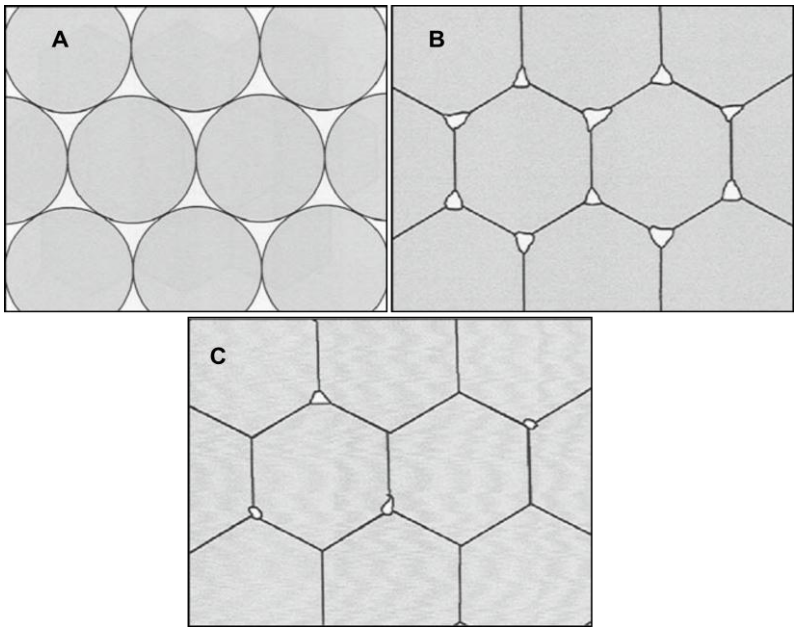

Figure 1. 4 – Zirconia sintering stages. A - Powder particles compacted together; B - Particles beginning to bind together; C- Fully sintered ceramic [8].

1.6. Zirconia Properties

Zirconia is a bioinert ceramic. This property classifies the material according to its reactivity with living tissues, where a bioinert material cannot form a direct bond with natural bone.

Bioinert ceramics are generally corrosion-resistant and wear resistant. They aren't significantly toxic, and don't induce serious inflammatory, and allergic reactions and also, these ceramics possess common ceramic characteristics such as hardness, low friction coefficient, and resistance to compressive stress [12].

Zirconia is highly biocompatible, has high mechanical strength, fracture toughness, good wear resistance, good resistance to corrosion and to chemicals and aesthetic appearance. However, some of zirconia drawbacks include the fact that it exhibits high density, low hardness, and phase transformations under stress in aqueous conditions, which can degrade their mechanical properties [5, 7]. Some values of mechanical properties of zirconia are shown below, in table 1.1.

Table 1. 1-Values of some mechanical properties of Yttria-Polycrystalline Tetragonal Zirconia. Adapted from [4].

Properties	Young´s modulus (GPa)	Flexural Strength (MPa)	Hardness (Vickers, HV0.5)	Fracture toughness (MPa/m2)	Weibull modulus	Density
Y-TZP **(Yttria-Polycrystalline Tetragonal Zirconia)**	210	950	1250	10,5	18	6

Although zirconia presents good mechanical properties, the fact that it is bioinert has prevented its use in the field of biomaterials and clinical devices in a wider way, as its limited use in dental implants. So, it is important to create new approaches that make possible its wider use. The use of bioactive coatings on zirconia substrates can be a good approach to allow a connection with the surrounding tissue in the oral cavity. Next, a technique to product silica bioactive thin films will be described.

2. Thin films production

2.1. Sol gel method for Silica Glasses

The **sol-gel** process is a wet-chemical technique widely used in materials science and ceramic engineering. It allows to produce glasses, ceramics, metals and polymers. This method is an attractive alternative for the synthesis of glasses for many reasons, as its low temperature, simplicity of required equipments, simple operation schemes, relatively low cost, low environmental impact and, of course, the properties of the obtained material [13].

In recent years, sol–gel process has been increasingly employed for the processing of bioactive glasses, including silica glasses.

The sol-gel process for glasses leads to the formation of gels from mixtures of liquid reagents (sols) at room temperatures. It involves several steps: the evolution of inorganic networks, formation of colloidal suspension (Sol) and gelation of the sol to form a network in a continuos liquid phase (Gel). Drying of the obtained gels, even at room temperature, produces glass-like materials called xerogels (xero-dry) [14, 15].

The sol-gel process for silica glass comprises several steps. First, a silicate precursor is mixed with a solvent and a catalyst and stirred for a few hours. This process leads to hydrolysis. The hydrolysis reaction can be catalyzed by acids (acetic acid, nitric acid, etc.) or alkalis (Sodium hydroxide, Ammonium hydroxide, etc.).

In the gelation process the sol transforms into a gel. This step consists in the establishment of bonds between the solution molecules to form a three dimensional network. It is important to stand out that this process is different from the solidification of a mixture, since the solid structure remains completely impregnated with the liquid of the sol [16].

During the **aging** step the sol-gel derived material expels the liquid phase (solvent) in the process called **syneresis** [14, 17]. The pore size of the material depends on factors such as time and temperature of the hydrolysis and kind of catalyst used. The average pore diameter is directly related to the shrinkage of the “wet” gels. During the **drying** process the gel volume decreases even several times (which is the main reason for cracking. After the drying process a glasslike material is obtained – Xerogel [14].

Finally, the material is heat-treated in order to favor further polycondensation and obtain a material with more adequate mechanical properties, lower pores sizes and structural stability via **sintering** and densification of the material. In the following scheme the general process to obtain a silica glass through Sol-gel technique is presented.

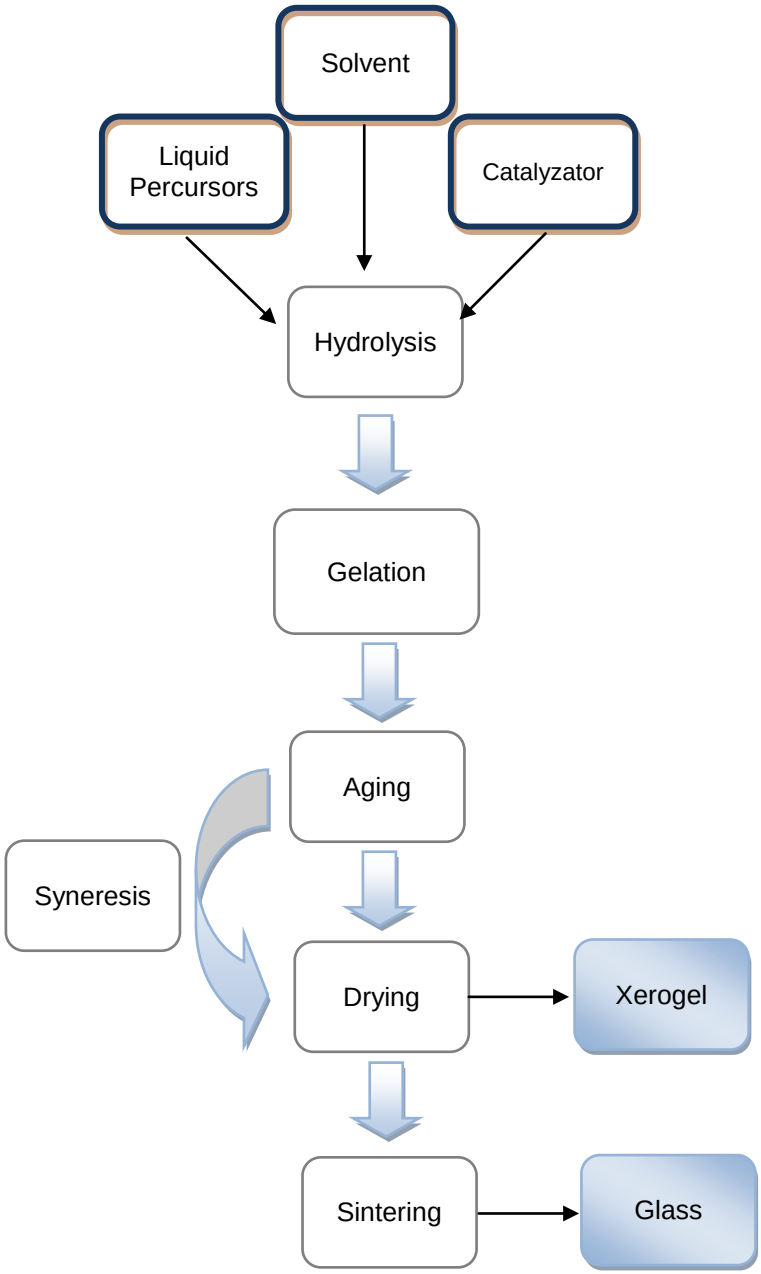

Figure 1. 5 – Summarizing scheme of Sol-gel technique for glass production. Adapted from [14].

2.2. Hybrid silica glasses

Hybrid glasses are obtained by adding organically-modified alcoxides to the sol. These precursors contain organic groups linked to silicon through a non-hydrolysable covalent bond. Hybrid coatings present critical thicknesses over 2 μm, much thicker than inorganic ones and with better mechanical properties. Organic groups affect the physicochemical properties at the pore surfaces, reducing drying stresses and

consequently the risk of cracking of the film. Methyltriethoxisilane (MTES) is one of the organically modified precursors most employed for the introduction of organic methyl groups. The MTES methyl groups act as network modifiers, reducing the connectivity, increasing plasticity and allowing for higher material densification. Therefore, high MTES contents lead to lower film shrinkage after thermal treatment, as well as to a higher film stability. This precursor usually is used together with Tetraethyl orthosilicate (TEOS) [18].

2.3. Advantages of Sol-gel method

There are several advantages of a sol–gel-derived glass over a melt-derived one, such as:

- Lower processing temperatures;
- The potential of improved purity, required for optimal bioactivity due to low processing temperatures and high silica and low alkali content;
- Improved homogeneity;
- Wider compositions ranges can be used (up to 90mol% SiO2) while maintaining bioactivity:
- Better bioactivity control by changing composition or microstructure;
- Structural variation can be produced without compositional changes by controlling hydrolysis and polycondensation reactions during synthesis;
- Increased bioactivity;
- Interconnected nanometer scale porosity that can be changed to control dissolution kinetics or be impregnated with biologically active phases such as growth factors;
- Can be foamed to provide interconnected pores of 10– 200 μm, mimicking the architecture of trabecular bone [16, 19, 20]

2.4. Thin films production

Manufacturing sol–gel derived coatings is a promising application of sol–gel technology, since a variety of coating materials can be applied on various substrates, such as metals, glasses and ceramics, and without expensive equipment. Furthermore, these coatings allow for improvement in the mechanical, thermal, protective, bioactive and electrical properties of the substrate material. Nowadays, many biomaterials are

coated with thin films to modify their surface and interface properties and many studies have been carried out in this area [13, 21]

Thin film formation by sol–gel method involves preparation of a sol, deposition of the sol onto a surface, formation of a gel state and drying of the gel. The surface of the substrate is coated, normally by a dip-coating or a spin-coating technique. The resulting film is dried at a temperature near room temperature to preserve the film porosity. Film thickness is determined by the withdrawal speed or spin speed in the case of dip and spin-coating [13, 17, 22]. The following figures (Figure 1.6 and figure 1.7) show the operations schemes of both dip and spin coating, respectively.

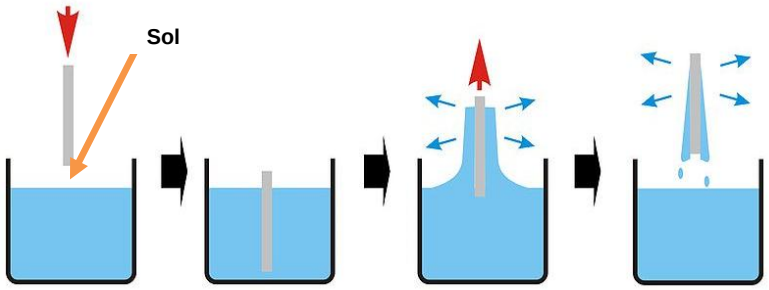

Figure 1. 6 - Scheme representing the dip-coating process. The stages of the dip coating process represented are: dipping of the substrate into the coating solution, wet layer formation by withdrawing the substrate, gelation and drying of the layer by solvent evaporation [23].

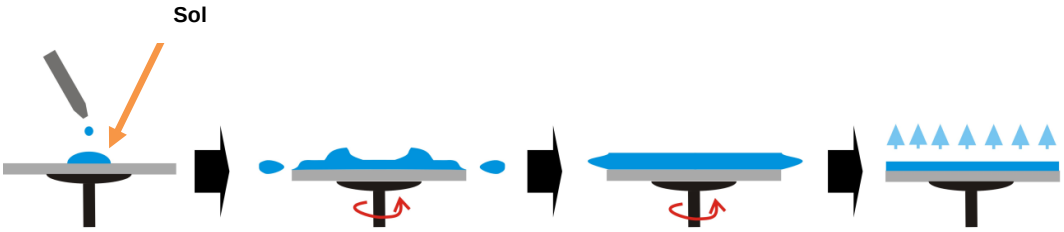

Figure 1. 7 - Scheme representing the spin-coating process. First, there is the deposition of the sol, then the spin-up in the spin coating machine and finally the gelation and drying by solvent evaporation [23].

2.5. Silica biological properties

The high biocompatibility and the positive biological effects of silica glasses and their reaction products (both leached or formed at the surface) after implantation, have made silica-based glasses one of the most interesting biomaterials during the last 40 years. This type of glasses is bioactive, binds to and interacts with living bone in the body without forming fibrous tissue around it nor promoting excessive inflammation or

toxicity, provides molecular control over the incorporation and biological behavior of proteins and cells, and provides osteoconductivity and osteointegration [16, 24-26]

So, due to the high surface area and porosity derived from the sol–gel process, the range of bioactive compositions is wide, also exhibiting high bone bonding rates together with excellent degradation/ resorption properties [27]. Sol–gel derived glasses also exhibit significant bioresorbability when their pores reach a particular size. Bioresorption is defined as the resorption of a material in vivo, due to the action of osteoclasts, which in this case is enhanced by the interconnected pore network, high surface areas and low particle density. These materials degrade gradually while the biological tissue is formed [20].

A common characteristic of all known bioactive materials is the formation of a biologically active hydroxycarbonated apatite (HCA) layer, due to surface dissolution, in a physiological environment. The higher the solubility of the glass, the more pronounced is the effect on bone tissue growth. In addition, degradation ionic products, especially silica species, have shown osteoconductive properties. This formation of HCA on bioactive glasses and the release of soluble silica and calcium ions to the surrounding tissue are key factors in the rapid bonding of these glasses to tissue, stimulating ~~of~~ tissue growth and application in tissue engineering scaffolds [16, 20, 26].

There are two classes of bioactivity. The silica glasses belong to the Class A bioactive materials. These materials show fast bone bonding, enhanced bone proliferation and, they also bind to soft connective tissues. Class A bioactive materials exhibit 11 reaction stages that lead to enhanced proliferation and differentiation of osteoblasts and recreation of trabecular bone architecture *in situ*. These are described below. Stages 1-5 are chemical and stages 6-11 are concerned to the biological response:

1. Rapid exchange of Na+ and Ca2+ with H+ or H3O+ from solution (diffusion controlled with t1/2 dependence, causing hydrolysis of the silica groups, which creates silanols);

$$Si{-}O{-}Na^{+} + H^{+} + OH^{-} \rightarrow Si{-}OH^{+} + Na^{+}_{(aq)} + OH^{-}$$

   The pH of the solution increases as a result of H^{+} ions in the solution being replaced by cations.

2. The cation exchange increases the hydroxyl concentration in solution, which leads to etching of the silica glass network. Soluble silica is lost to the

solution as $Si(OH)_4$ resulting from the breaking of Si-O-Si bonds and the continued formation of Si-OH (silanols) at the glass solution interface:

$$Si-O-Si+H_2O \rightarrow Si-OH+OH-Si$$

This stage is an interface-controlled reaction with a $t^{1.0}$ dependence.

3. Condensation and re-polymerization of a SiO_2-rich layer on the surface, depleted in alkalis and alkali-earth cations.
4. Migration of Ca^{2+} and PO_4^{3-} groups to the surface through the SiO_2-rich layer, forming a $CaO-P_2O_5$-rich film on top of the SiO_2-rich layer, followed by growth of the amorphous $CaO-P_2O_5$ -rich film by incorporation of soluble calcium and phosphates from solution.
5. Crystallization of the amorphous $CaO-P_2O_5$ film by incorporation of OH^- and CO_3^{2-} anions from solution to form a mixed hydroxyl carbonate apatite (HCA) layer.
6. Adsorption and desorption of biological growth factors, in the HCA layer (continues throughout the process), to activate differentiation of stem cells.
7. Action of macrophages to remove debris from the site allowing cells to occupy the space.
8. Attachment of stem cells on the bioactive surface.
9. Differentiation of stem cells to form bone growing cells osteoblasts.
10. Generation of extracellular matrix by the osteoblasts to form bone
11. Crystallization of inorganic calcium phosphate matrix to enclose bone cells in a living composite structure [16, 20, 26].

2.6. Addition of Nanoparticles

Ceramic nanoparticles can be added to the silica thin films in order to increase bioactivity and contact surface area. Hydroxyapatite (HA) has been widely used as a biocompatible ceramic in many areas of medicine, but mainly for contact with bone tissue. HA possesses exceptional biocompatibility, bioactivity and osteoconductive properties with respect to bone cells and tissues, probably due to its similarity with the hard tissues of the body [28, 29].

Compared to conventional ceramic formulations, nanophase HA properties such as surface grain size, pore size, wettability, etc, could control protein interactions (for

example, adsorption, configuration and bioactivity); therefore, modulating subsequent enhanced osteoblast adhesion and long-term functionality. Previous studies discovered that these enhanced osteoblast functions are proliferation, alkaline phosphatase synthesis and calcium containing mineral deposition. Nanometer grain size topography and surface wettability are nanoceramic material properties that not only promote increased selective vitronectin adsorption (a protein that mediates osteoblast adhesion) but also affect conformations that enhance osteoblast functions [28, 30, 31].

3. Micropatterning

3.1. Micropatterning Aspects

Topographic modulation of tissue response can be one of the most important considerations during the design and manufacture of a biomaterial. If tissue and cell types differ in their response to topographic variations, this phenomenon may be exploited to design implant materials.

Surface microfabrication techniques have been widely utilized for the spatial control of cells in culture. Many strategies have employed changes in surface charge, hydrophilicity, and topology to regulate cell functions such as attachment. The surface-patterning techniques enabled visualization of the effect of surface properties on cell functionality and spatial control of cellular micro-organization [32, 33].

Among the strategies to modify implant surfaces is **micropatterning.** This technique, allied to sol-gel method provides promising and cost-effective micropatterning processes. The general aspects of this technique are that an initially liquid/gel is allowed to acquire its final geometry by solidifying in a mold. This technique allows the reproduction of the mold fine details. The molds may have structures with tens of nanometer size features and can be generated in elastic polymers such as polydimethylsiloxane (PDMS).The micropatterning method can be used to produce micropatterns even on curved substrates. Although, it is important that in the molding process the solution covers the surface of the substrate and allows the contact of the elastic stamp with the substrate. The patterning required in microfabrication is usually carried out by photolithography. Although it is difficult to find a better technology, photolithography nonetheless has disadvantages. The size of the features that it can produce is limited by optical diffraction, and the high-energy radiation needed for small features requires complex facilities and technologies. Photolithography is an expensive technique, it cannot be easily applied to non-planar surfaces and it provides almost no control over the chemistry of patterned surfaces, especially when complex organic functional groups of the sorts required in chemistry, biochemistry, and biology are involved [34-36].

3.2. Soft-Lithography

Soft-lithography is a general term for a variety of techniques, all of them employing an elastomeric (PDMS) mold to develop patterns on a planar surface.

Micropatterning by soft-lithography as a bench type processing technique is remarkable for its economy and simplicity, as well as for its potential to produce a variety of surface patterns or modifications without the complex masks and steps required in optical lithography. Soft-lithography techniques can be used to develop both two-dimensional surface patterns as thin films or SAMs, as well as to generate quasi three-dimensional topographical features. Soft-lithography can produce micro and nano-features arranged in an organized manner (isotropic) or in a random manner (anisotropic) [33, 36]. A schematic figure of the soft-lithography process is shown bellow in figure 1.8.

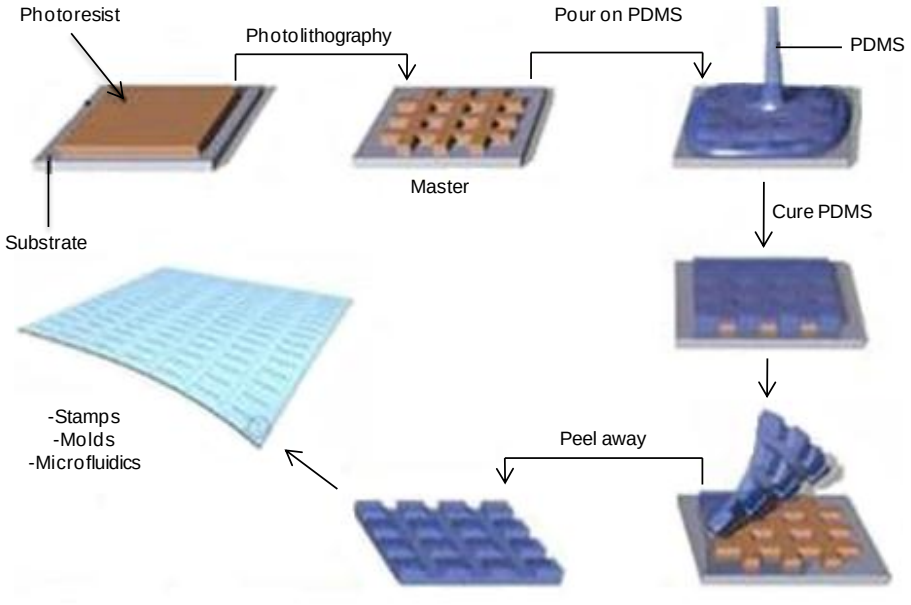

Figure 1. 8 - Soft–Lithography process to obtain a final elastomeric negative mold with the desired pattern. Adapted from [37].

In soft-lithography, a master with the desired features is first prepared by photolithography. The micropatterned PDMS mold is then prepared by casting a liquid pre-polymeric mixture on a wafer master containing the designed pattern. The mixture is left curing, and finally the PDMS is peeled off the master to obtain the finished negative mold [33].

After preparation the PDMS mold is used to stamp a solution on a chosen substrate. Associated with the sol-gel method, two techniques to microstamp a substrate are highlighted: **microtransfer molding** (μTm) and **micromolding in capillaries** (MIMIC) [35, 36]. A schematic figure of the method of processing of these techniques is shown bellow (Fig. 1.9)

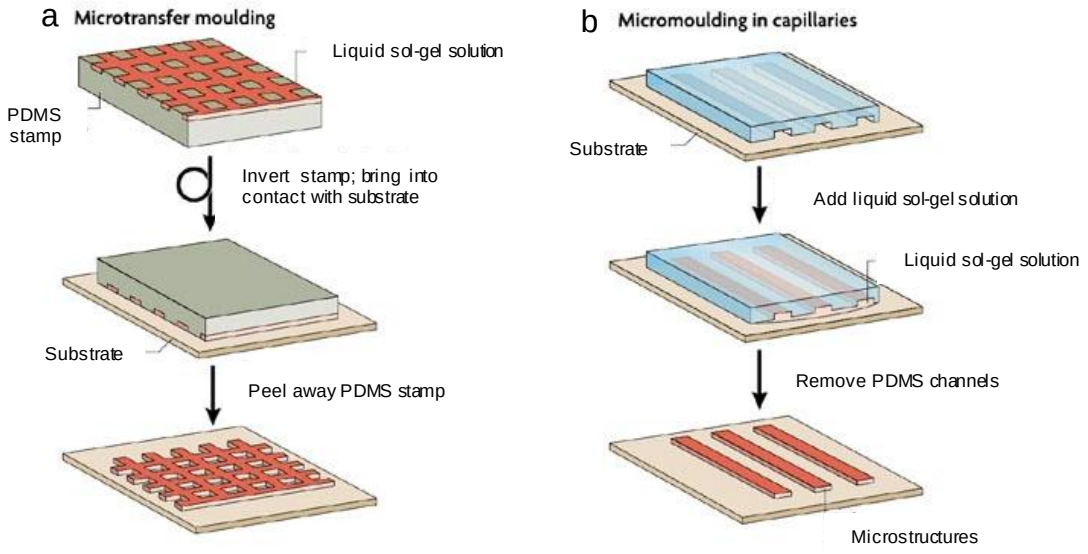

Figure 1. 9 - Two microstamping techniques associating soft-lithography and solutions prepared by sol-gel method. a) Microtransfer molding and b) Micromolding in capillaries. Adapted from [38].

In the micro-transfer molding technique (Fig. 1.9 *a*), a small amount of the sol-gel solution is deposited onto the patterned surface of the PDMS mold so it fills the relief. After removing any excess of sol-gel solution, the filled mold is placed in contact with the substrate, and following curing, the PDMS mold is removed leaving a deposited pattern of the sol-gel. By using this technique, isolated features can be generated on the substrate. In what concerns to the micromolding in capillaries, the clean PDMS mold is first sealed against the glass surface. The sol-gel solution is then deposited at the open ends of the PDMS mold, and capillary action allows infiltration of the sol-gel solution into the micro channel patterns. After in situ curing and removal of the PDMS mold, the patterned structure remains on the surface (Fig. 1.9 b) [35, 36].

3.3. Cell behavior

The structural organization of tissues plays a major part in deciding the degree and direction of tissue growth and cell movement: an effect often termed **'contact guidance'**. Various studies have indicated that it may be possible to design the surface texture of implanted materials to improve the performance of an implant [33].

Biocompatibility of soft-tissue implants is often hampered by the development of capsules that eventually might contrast and impair implant function. It has been shown that capsule formation can be significantly reduced by using materials with textured

surface elements in the micron and nano range [32, 33]. Topographic modulation of tissue response can be one of the most important considerations during the design and manufacture of a biomaterial [32]. There are several approaches using patterned surfaces that show improved cellular activity and enhancement of extracellular matrix synthesis of adherent cells, providing a faster and more reliable osteointegration response [39-41]. There is clear evidence that cell adhesion, proliferation, organization and phenotype are modulated at the micro-scale [42]. These effects arise from the increased adhesion of connective tissue cells onto the roughened surfaces, resulting in closer tissue apposition onto to the implant. Recent advances have shown that we are only in the beginning of understanding the importance of controlled cellular microenvironments and that the application of microfabrication approaches to study cell biology has opened up many and new interesting avenues for research [43].

The following figure shows the effect of nanotopography in cell behavior.

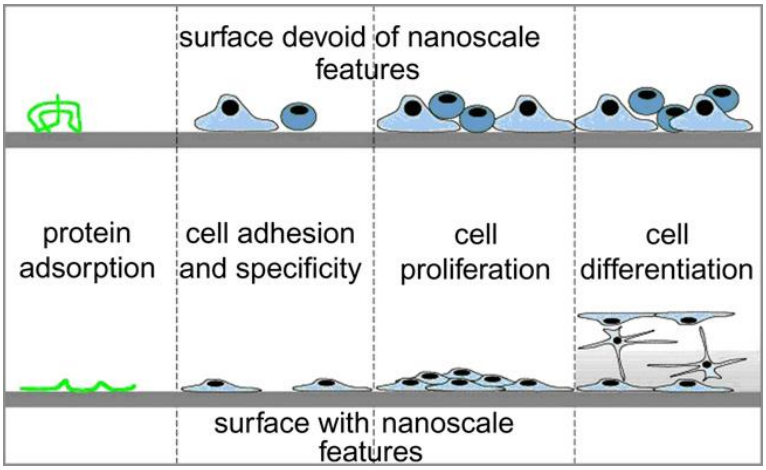

Figure 1. 10 - Depiction of broad range of nanoscale topography effects observed in cellular and protein adsorption. Both cell specificity and extent of cell adhesion are altered. Depending on the nano-architecture cell spreading may be increased or decreased. By presently undefined mechanisms, cell proliferation appears to be enhanced by nanoscale topography [33].

4. Mesenchymal Stem Cells and Bone Remodeling

4.1. Mesenchymal Stem Cells

Mesenchymal Stem Cells (MSCs) are a heterogeneous group of progenitor cells with pluripotent capacity to differentiate into several connective tissue cell types, including osteoblasts, chondrocytes, adipocytes, tenocytes and myocytes (figure 1.11) [44, 45]. MSCs were first identified in bone marrow but since then they have been isolated and identified in many other tissues including adipose tissue, umbilical cord blood, muscle, dental pulp, amniotic fluid and skin [46, 47].

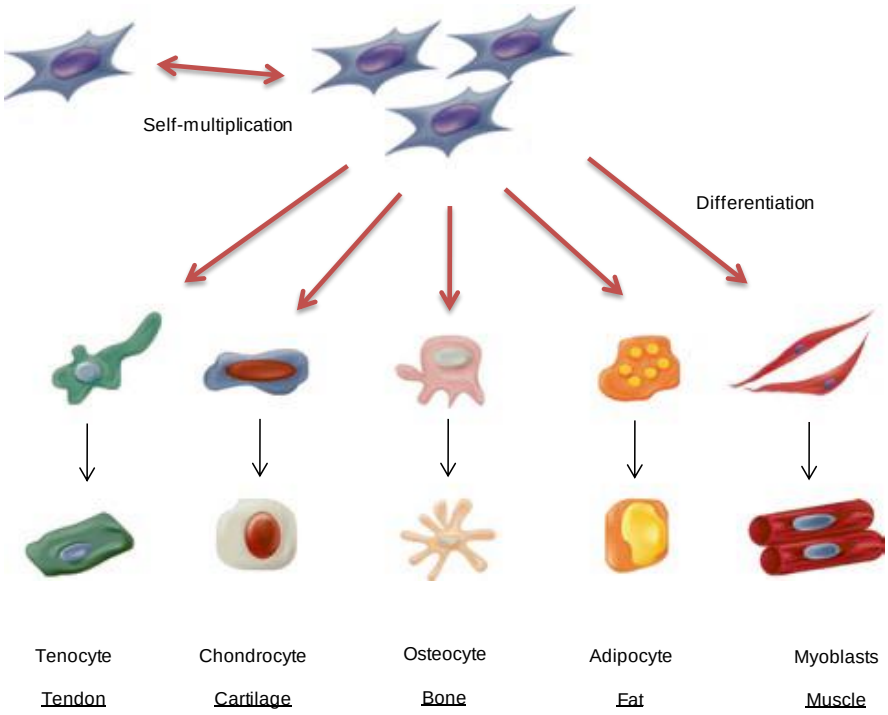

Figure 1. 11 - Multilineage differentiation potential of mesenchymal stem cells (MSCs). Adapted from [48].

The isolation of MSCs from these various tissues usually involves adherence of the cells to tissue culture plastic, with or without subfractionation or enrichment strategies. The three main criteria to identify a MSC population are the adherence to tissue culture plastic under standard culture conditions, cell surface characterization by cell surface antigens and *in vitro* tri-lineage mesoderm differentiation [47, 48].

Human MSCs have been defined by the positive expression of the cell surface antigens including CD73, CD90, CD105 and a lack of expression of hematopoietic antigens including CD11b or CD14, CD34, CD45, CD79 or CD19, and HLA-DR [48].

Under appropriate conditions, MSCs are able to differentiate into cell types of different lineages, *in vitro.* For example, incubating MSCs with ascorbic acid, beta-

glycerophosphate and dexamethasone for 2-3 weeks induces osteogenic differentiation [45]. After this time of culture, bone cells can easily be identified.

The morphological and histological criteria by which osteoblastic cells, including osteoprogenitors, pre-osteoblasts, osteoblasts, and lining cells or osteocytes, are identified have been reviewed extensively. Morphological definitions are now routinely supplemented by the analysis of the expression of cell- and tissue-specific macromolecules, including the ecto-enzyme ALP, bone matrix proteins like type I collagen (COLL-I), osteocalcin (OCN), OPN, and bone sialoprotein (BSP) and transcription factors that regulate them and the differentiation events (Runx2, AP-1 family members, Msx-2, Dlx-5, etc.) [47].

4.2. Dental Pulp Stem Cells

Dental Pulp Stem Cells are one type of mesenchymal stem cells that can be obtained from the dental pulp, a soft connective tissue entrapped within the dental crown that is an extremely rich site for stem cell collection. In addition to nerves and blood vessels, the pulp contains highly proliferative stem cells possessing a self-renewal and differentiation capability. Owing to its peculiar formation, the pulp chamber is a sort of ‘‘sealed niche’’ and may explain why it is possible to find a rather large number of stem cell there (figure 1.12) [49-51].

During the sixth week of embryogenesis, the ectoderm covering the stomodeum begins to proliferate, giving rise to the dental laminae. Ectoderm–mesoderm interactions then lead to placode formation. One of these ovoidal ectodermal structures develops into tooth germs, where neural crest cells differentiate into the dental organ, dental papilla and dental follicle. Therefore, dental pulp is made of both ectodermic and mesenchymal components, containing neural crest cells that display plasticity and multipotential capability [49].

A series of studies have shown that DPSC provide characteristic stem cell properties as they are self-renewed, highly proliferative with clonogenic efficiency, and possess the capability for multi-lineage differentiation [50].

This type of stem cells was first isolated by Gronthos and colleagues, in 2000. Since then, they have been studied for several favorable reasons, such as easy surgical access, the high efficiency of the extraction procedure of the stem cells from the pulp tissue, their differentiation ability and proved interactivity with biomaterials for tissue engineering [51].

In 2005, the group of Laino and Papaccio isolated a selected population of dental pulp stem cells called SBP-DPSCs, which were already capable of woven bone tissue

formation *in vitro*. Experiments performed with SBP-DPSCs confirmed that bone was the main commitment of dental pulp stem cells, from the expression RUNX-2, a transcription factor involved in the inducing of osteoblast differentiation. Laino and colleagues also demonstrated that this type of cells, when undergo their differentiation to preosteoblasts, deposit an extracellular matrix which becomes a calcified woven bone tissue called LAB (living autologous bone) that can be produced already *in vitro,* in 3D scaffolds. Upon transplantation in vivo, the tissue is actually remodeled to form a lamellar bone through co-differentiation of SBP-DPSC into osteoblasts and endotheliocytes. During the in vitro ossification process, the SBP-DPSCs cells give rise to both osteoblasts and endotheliocytes, and to bone containing vessels, leading to the formation of an adult bone tissue after in vivo transplantation. The presence of these vessels and their complete integration with host, other than being the demonstration of a complete tissue growth from stem cells, is of great importance for its use in therapy [51, 52].

Due to their high proliferation rate and efficiency in producing bone chips, DPSCs seem to be the best candidates to study bone formation with respect to bone marrow stem cells (BMSCs), whose efficiency is limited by the fact that they differentiate into osteoblasts and produce small calcified nodule, but not chips of bone tissue. In this way in pre-clinical phase it is possible to assess the osteoconductivity of a biomaterial [51].

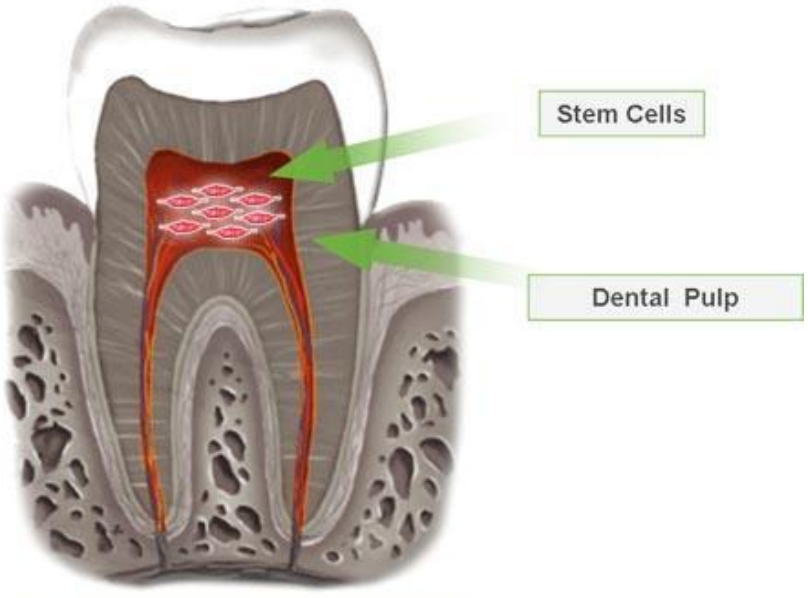

Figure 1. 12 - Collection site of dental pulp stem cells from the dental pulp [53].

4.3. Bone Remodeling

Bone contains four types of cells: osteoprogenitor cells, osteoblasts, osteocytes, and osteoclasts, of which osteocytes are the most abundant. In general osteoblasts are cells that create new bone, and osteoclasts are cells that destroy it when force is applied [54, 55].

Understanding the process of bone remodeling is of paramount importance in implant design and materials selection [4]. Bone is first resorbed by osteoclasts and then formed at the same site by osteoblasts. These cells form the basic metabolic unit (BMU) that reconstructs bone. Bone modeling and remodeling achieve strength for loading and lightness for mobility in two ways: by strategically depositing bone in locations where it is needed to modify bone size and shape, and by removing bone from where it is not needed to avoid bulk [56, 47]. Bone remodeling can be separated into two categories; surface and internal remodeling. **Surface remodeling** is the resorption and deposition of bone material on the external surfaces of bone (periosteal surfaces), while **internal remodeling** is reinforcement and resorption in the endosteal surfaces, resulting in changes in the bulk density of the bone [4, 56].

Bone remodeling involves four main processes: activation, resorption, reversal and formation. The remodeling cycle is initiated by the activation of the quiescent bone surface, which is covered with bone lining cells. Osteoclast precursor cells are recruited to the activated surface and fuse to form mature, bone resorbing osteoclasts. The osteoclasts attach to the surface and dissolve the inorganic matrix by creating an acidic microenvironment and degrade the organic matrix with specific enzymes. As bone resorption subsides and resorption pits remain osteoclasts disappear and mononuclear cells prepare the surface for bone formation. Also, osteoclasts phagocytose osteocytes and this may be one way the signal for resorption is removed. Products from the osteoclasts independent of their resorption activity, and products from the resorbed matrix partly regulate osteoblastogenesis and bone formation. The bone remodeling cycle is finished with the synthesis and deposition of bone matrix by osteoblasts, where some differentiate to bone lining cells building a canopy covering the surface keeping the material dormant until the next cycle and others become entombed in the bone matrix and become osteocytes [55, 57].

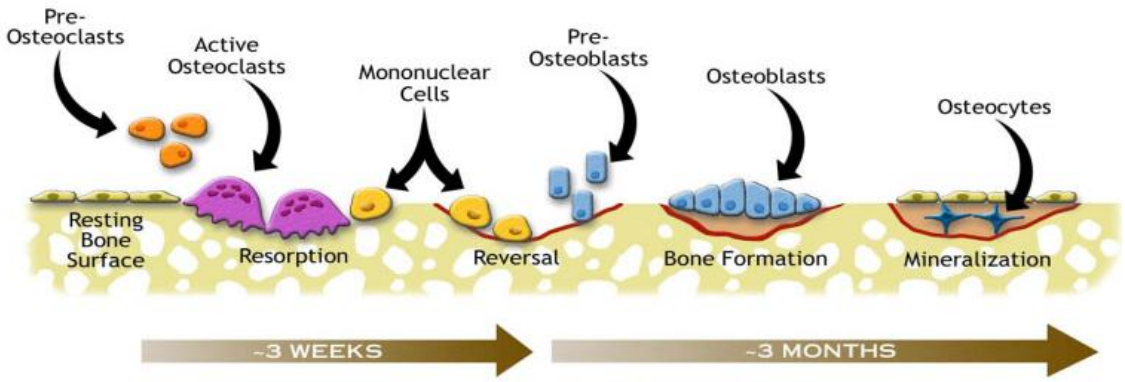

Figure 1. 13 - Cycle of bone remodeling [58].

5. Oral Infections

5.1. Infections

The implantation of a biomaterial into the human body, and the subsequent damage caused to the tissues is known to increase susceptibility to infection [59]. Nowadays, device-related bacterial infections are one of the greatest challenges to the more widespread application of medical implants [60]. Microbial adhesion to surfaces and the formation of a complex biofilm at the interface between a biomaterial and the biological environment are frequent reasons for the failure of biomaterial devices [59].

Infection represents one of many factors contributing to the failure of dental implants. The oral cavity is a unique environment, as different types of surfaces (hard, soft, natural and artificial) share the same ecological niche. In order to survive within this 'open growth system' and to withstand shear forces, bacteria need to adhere either to soft or to hard tissues. The initial adhesion and the successful colonization of bacteria onto solid surfaces play a key role in biofilm formation and in the pathogenesis of infections related to biomaterials [61, 62].

Clearly, controlling this initial adhesion into a biofilm depends mainly on the surface properties. While several dental materials promote selective adherence during early dental biofilm formation, other modified biomaterials may provide resistance to bacterial adhesion and biofilm formation [62].

A biofilm is a layer-like aggregate of cells and cellular products attached to a solid surface or substratum. An established biofilm structure is made up of microbial cells and extracellular polymeric substances and provides an environment for the exchange of genetic material between cells. Within biofilms, microorganisms organize communities with structural and functional heterogeneity similar to that of a multicellular organism; interstitial voids between micro-colonies can be considered to serve as a rudimentary circulatory system. Cell-to-cell signaling (i.e. quorum-sensing) induces biofilm microorganisms to change patterns of gene expression. Quorum-sensing is the ability of a bacterial colony to sense its size and in response to regulate its activity. At a certain population density, intercellular signals activate genes involved in biofilm differentiation [63]. The next figure (Fig.1.14) shows the processes to a biofilm formation.

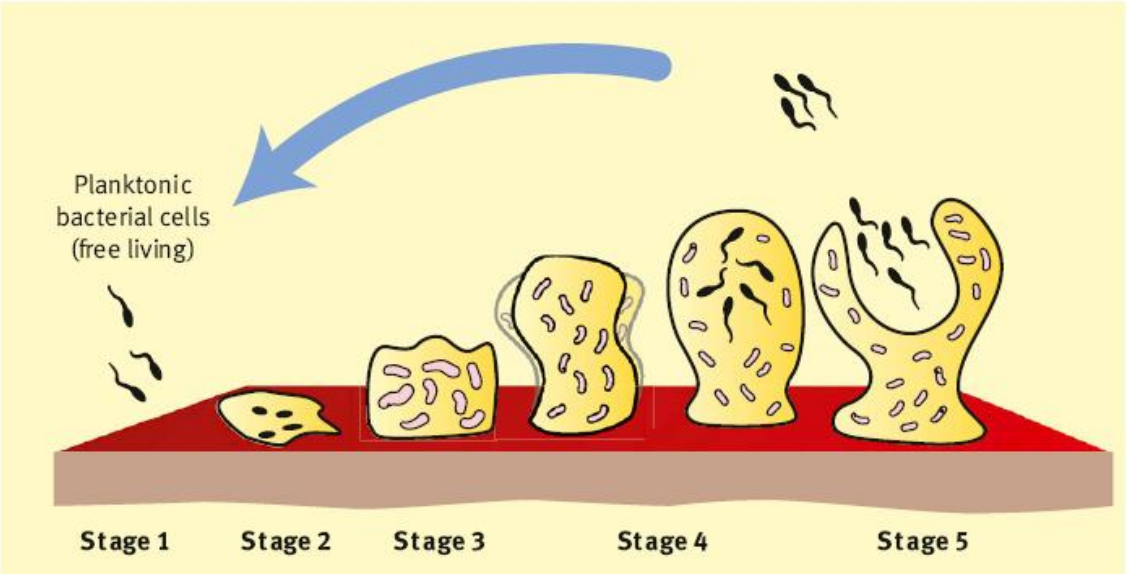

Figure 1. 14 - Diagram showing the development of a biofilm as a five-stage process where, stage 1: initial attachment of cells to the surface. Stage 2: production of extracellular polymeric substance. Stage 3: early development of biofilm architecture (colonization). Stage 4: maturation of biofilm architecture. Stage 5: dispersion of single cells from the biofilm. In the final stage, when environmental conditions become unfavorable, some of the bacteria may detach and swim away to find a surface in a more favorable environment [63].

5.2. Bacteria causing the infection

Although the mechanism of bacterial infections with implants is not well understood, the microflora around dental implants appear to be similar to that found around natural teeth. So, microbial pathogens associated with periodontitis may also contribute to implant failure [64].

Between the main microorganisms present in oral cavity, usually related to various infections, are *Porphyromonas gingivalis* and *Streptococci mutans*. Along the years, various studies have shown presence of these two bacteria in infected dental implants, although there is not much information about these interactions [65, 66].

Porphyromonas gingivalis is a gram-negative anaerobic that is widely recognized as a predominant contributor to human periodontitis. This is a polymicrobial infection-driven inflammatory disease of the oral cavity, characterized by chronicity and destruction of the tooth-supporting tissues [67]. In dental implants is normally associated with peri-implantitis [68].

When peri-implantitis is prolonged, the alveolar bone that supports the implant may be degraded and the implant fails. When this happens it becomes very difficult to replace the implant. Figure 1.15 shows a comparison between a healthy tooth and one with a periodontal disease.

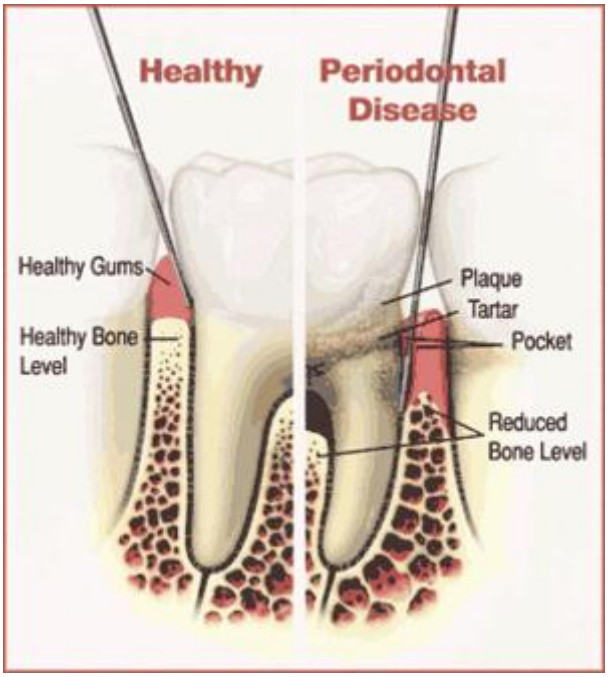

Figure 1. 15 - Comparison between a healthy tooth and a tooth with peridontal disease [69].

P. gingivalis is thought to spread through tissue, destroy it, and evade host defenses by the use of secreted cell-bound proteases, immunoactive cellular compounds, and toxins. *P. gingivalis* cytotoxic metabolic end products, which include butyrate, propionate, have low molecular weights which allows them to easily penetrate periodontal tissue and disrupt the host cell activity [70].

Other bacteria commonly associated with dental infections are *Streptococcus mutans*. Previous studies have indicated that S*treptococci mutans* are the predominant colonizing micro-organisms of oral surfaces. *S. mutans* is considered to be a most important etiological agent of diseases associated with dental caries. On teeth, it is one of the species that form biofilm causing dissolution of enamel by acid end-products resulting from carbohydrate metabolism [62]. *Streptococcus mutans* is a Gram-positive bacterium that metabolizes different kinds of carbohydrates, creating acidic environment in the mouth as a result of this process. This acidic environment in the mouth is what causes the tooth decay. Associated with implants, it is thought that this bacterium can create an acidic environment that degrades the implant surface, provoking corrosion of the implant surface, although not much is known about this biological interaction [66, 71].

II. Materials and Methods

1. Materials Preparation

1.1. Silica preparation

Zirconia discs were prepared using a centrifuge assisted casting method; however it was very difficult to reproduce the coatings in the zirconia surface in large scale. So, since a high number of samples was required to perform all the characterization tests in the thin films, another material that would allow higher reproducibility (glass) was used as substrate. This way, in this study glass coverslips with 15 mm diameter were used as substrates to evaluate the silica flat and micropatterned thin films.

Hybrid silica sols were produced via sol-gel process with acid catalysis in a single stage. Tetraethylorthosilicate (TEOS, Sigma-Aldrich) and Methyltriethoxisilane (MTES, Sigma-Aldrich) were used as silica sols precursors in a ratio of 40:60, respectively. Alcohol was used as a solvent and acetic and nitric acids were used as catalysts.

The flat SiO_2 coatings were applied on glass cover slips by spin-coating for 45s at 3000rpm.

1.2. Molds preparation

Soft-lithography was used to produce the molds with the microscale features by a two-step process. First, photolithography was used to produce master pattern with micro-scale dimensions. The master was then used to create polydimethylsiloxane (PDMS) negative molds. PDMS (Silastic T-2, Dow Corning, USA) was uniformly mixed with a curing agent, deposit into the master, degassed and cured. The final negative molds were then used to stamp the samples and create the micropattern. Figure 2.1 shows the complete soft-lithography process since the wafer production to the stamping step.

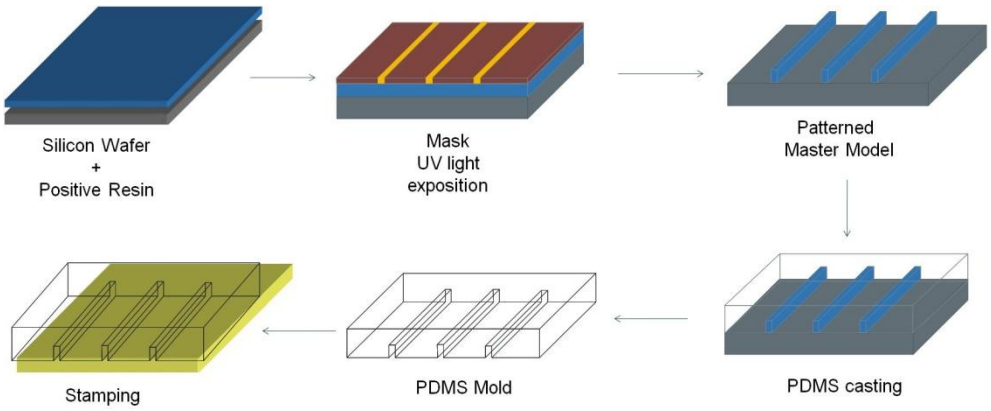

Figure 2. 1 – Soft-lithography method used to create micropatterned PDMS molds.

1.3. Microstamping

Three types of microfabricated silica thin films were produced. Nanoscale hydroxyapatite (nanoHA) particles were introduced into the sol for incorporation into the thin films at two difference weight ratios (1 and 5%) and the silica sol was also used solo. The microfabricated coatings were obtained by single molding (Figure 2.2) by applying 40 µl of the silica mixtures in the glass coverslips and pressing with the PDMS mold after. This was left drying overnight and after the PDMS mold was removed, as shown in figure 2.2.

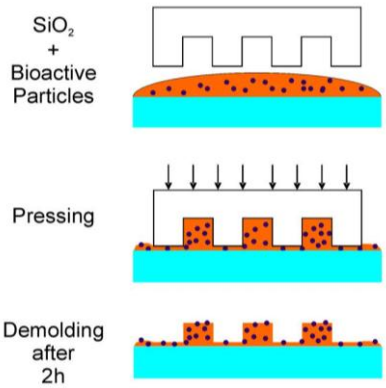

Figure 2. 2 – Stamping procedure by single molding method.

1.4. Sintering

Samples were sintered at 500ºC for 60 minutes, using the sintering cycle shown in figure 2.3.

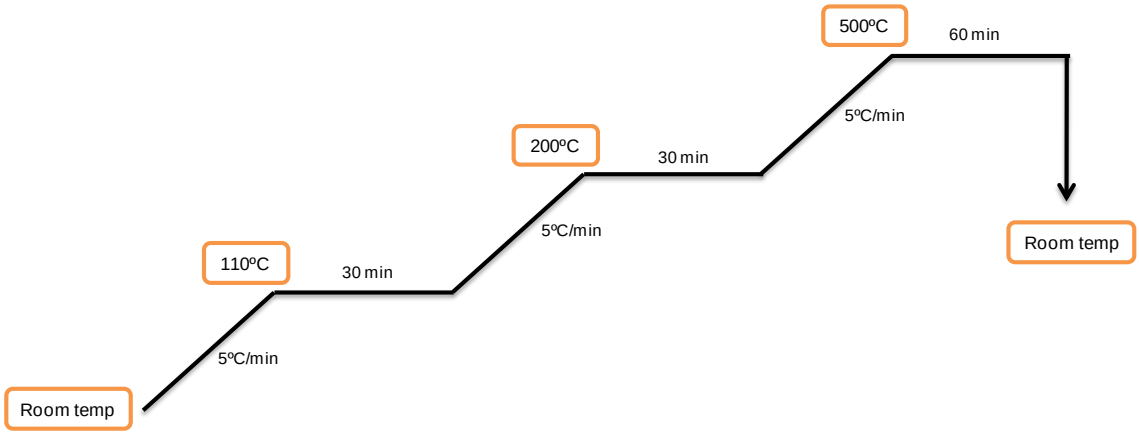

Figure 2. 3 – Sintering cycle used to sinter the silica thin films.

2. *Surface characterization*

After the heat-treatment, the samples were evaluated under light microscopy and the surface was characterized.

2.1. *Scanning Electron Microscopy* / Energy Dispersive X-ray Spectroscopy

Scanning Electron Microscopy (SEM) and Energy Dispersive X-ray Spectroscopy (EDS) evaluations were carried out with a FEI Quanta 400FEG ESEM / EDAX Genesis X4M scanning electron microscope at 15KeV. The samples were sputter-coated with palladium-gold.

2.2. *Contact Angle*

The contact angle measurements were performed using equipment from Data physics Instruments GmbH, Germany, model OCA 15 with a video device camera, an electronic syringe unit (Hamilton) and a SCA 20 software. The sessile drop method was used with ultrapure water at 25ºC in a chamber saturated with the same liquid. The contact angle was calculated by the Laplace-Young function when the drop contacted with the material surface. Since three of the materials have patterns, all were similarly oriented in order to maintain the same conditions to all the samples during all the experiment. The results expressed are the arithmetic mean ± standard deviation.

2.3. X-Ray photoelectron spectroscopy analysis

X-Ray photoelectron spectroscopy (XPS) was used for the elemental percentage analysis of the various surfaces and was carried out with a VG Scientific ESCALAB 200A. The various surfaces were analyzed within a depth of 5nm.

3. In vitro biological studies

To perform the in vitro biological studies the samples were sterilized with ethanol 70% during 30 minutes and washed with PBS twice afterwards.

3.1. Basal conditions cell culture

Human pulp derived mesenchymal stem cells in the second passage were cultured in α-minimal essential medium (α-MEM) containing 10% of fetal bovine serum and 1% of penincilin (10µg/ml), streptomycin (10IU/ml), fungizone (2,5µg/ml) and ascorbic acid (50µg/ml). The cultures were incubated in a humidified atmosphere of 5% CO_2 at 37ºC and the medium was changed three times a week. Cells were maintained until near confluence and the adherent cells were washed with phosphate buffered saline (PBS; Gibco, UK) and enzymatically released with 0.04% trypsin at 37ºC for 4 minutes and counted using a hemocytometer. The resultant cells were seeded at a density of 10^4 cells/cm^2 on the silica coated micropatterned samples (SiO_2, SiO_2 + 1% nanoHA and SiO_2 + 5% nanoHA) and on tissue culture polystyrene (TCP) to act as positive control, in 24-well plates. All cultures were incubated for 3 different time points (1, 7 and 14 days). At each time point, cells metabolic activity was evaluated using rezasurin and after washed twice with warmed PBS and fixed in 10% v/v neutral buffered Formalin (Sigma, USA) for 15min. The samples were then morphologically evaluated by fluorescence microscopy and scanning electron microscopy (SEM).

3.1.1. Metabolic activity

The alamar blue assay was used to determine the viability and proliferation of the cells, since it is a simple and non-reactive assay, were a non-fluorescent blue component is reduced by the living cells to a pink fluorescent component. Fresh medium with 10% of rezasurin was added to the cells and incubated for 3 hours. Afterwards, 100µl were transferred to a 96-well plate and the fluorescence was quantified in a microplate reader (Synergy HT, BioTek) at 535nm excitation wavelength and 590nm emission wavelength. The results were expressed in relative fluorescence units (RFU).

3.1.2. Morphology

For morphology evaluation with fluorescence microscopy (Zeiss Axiovert 200M) cells were washed and permeabilized with 0.1% v/v Triton X-100 (Sigma, USA) for 30 minutes. The cells F-actin filaments were stained using Alexafluor phalloidin (Invitrogen, USA) for 30 min and the nucleus were stained with a buffer of Propidium iodide and RNase (BD Pharmigen, USA) for 10 min and washed with PBS.

For the morphology evaluation via SEM, the cells were dehydrated in graded ethanol solutions and hexamethyldisilazane (HMDS, Ted Pella, USA) solutions from 50% to 100%, respectively. The samples were then sputter-coated with palladium-gold.

3.2. MSCs Osteogenic differentiation

A cell culture under osteogenic conditions was carried out to evaluate the potential of the human pulp derived MSCs to differentiate into osteoblasts.
MSCs in the 2ª passage were culture in the same conditions described in 2.1., After the release of the adherent cells with 0.04% of trypsin, the resultant cells were seeded in 96-well plates at a density of 10^4 cm^2. To one culture was added 1% of dexamethasone (10^{-8} M) and β-glycerophosphate (10^{-2} M) for osteogenic differentiation while the other continued with same conditions, for comparison. Both cultures were incubated for 4 different time points (4, 7, 14 and 21 days). At each time point, metabolic activity and alkaline phosphatase (ALP) activity and total protein content were measured.

3.2.1. Metabolic activity

Cells metabolic activity was measured at each time point as described in 3.1.1.

3.2.2. Alkaline phosphate activity and total protein content

For the alkaline phosphatase (ALP) activity and total protein content measurements, cells were washed with PBS, frozen at -20º and later thawed at 37º to carry on the measurements. Cells were permeabilized by adding 200µl of 0.1% v/v Triton X-100 for 30 minutes. Total protein was quantified by Lowry's method using Bovine serum albumin as a standard. Cells ALP activity was analyzed by substrate hydrolysis (p-nitrophenyl phosphate) in alkaline buffer solution (2-amino-2-methyl-1-propanol) at pH 10.5. The plate was incubated at 37º for 1h and consecutively NaOH (1M) was added to stop the hydrolysis reaction and the product p-nitrophenol was measured in a plate reader at 405nm of absorbance. The ALP results were normalized to total protein

content and were expressed in nanomoles of p-nitrophenol produced per minute and per microgram of protein (nmol $^{-1}$ ug protein $^{-1}$).

3.3. Osteogenic conditions cell culture

For the cell culture with osteogenic conditions, human pulp derived mesenchymal stem cells in the 3rd passage were cultured as described in 3.1.1. After the enzymatic release with 0.04% trypsin, the resultant cells were seeded at a density of $2x10^4$ on the materials - flat SiO_2, micropatterned SiO_2, SiO_2 + 1% nanoHA and SiO_2 + 5% nanoHA and TCP – in 24-well plates. All cultures were incubated for 4 different time points (1, 7, 14 and 21 days). From the third day of culture, cell medium was supplemented with 1% of dexamethasone (10^{-8} M) and β-glycerophosphate (10^{-2} M). During the times of culture the following tests were performed.

3.3.1. Metabolic activity

At each time point, cells metabolic activity was evaluated as described in 3.1.1. and after washed twice with warmed PBS and fixed in 10% v/v neutral buffered Formalin for 15min.

3.3.2. Alkaline Phosphatase Activity

ALP activity was measured at days 7, 14 and 21 using the protocol described in 3.2.1.

3.3.3. Morphology

SEM and Confocal Laser Scanning Microscopy (CLSM, Leica TCP SP2 AOBS) were used to observe cells morphology at each time point. Samples were prepared as described in 3.1.2.

3.3.4. Alizarin Red Staining

Alizarin red staining was used to access calcium-rich deposits produced by cells in culture. A solution with pH 6.3 was produced by mixing 3 mg of Alizarin Red S with 3ml of NH_4OH 0.28%. This solution was filtered and applied in the fixed cells for 2 min. After, cells were washed with distilled water and a solution of acid ethanol was added for 15 s. Cells were washed with distilled water again and left drying. This reaction stains the calcium deposits in orange/red. The stained samples were analyzed in a magnifying glass and an image of each was captured.
Since two of the materials contain nanoHA particles, a control of each one of these materials was also stained.

3.3.5. Reverse transcriptase polymerase chain reaction (RT-PCR)

RT-PCR was used to assess Runx2 gene expression, a transcription factor that is specifically required for osteoblast differentiation [72]. Total RNA was isolated from the cell culture on the materials using the RiboPureTM kit according to the manufacturer's instructions. RNA was quantified by measuring the absorbance of the samples at 260 nm. RT-PCR was performed using the Titan One Tube RT-PCR System (Roche Applied Science, USA), according to the manufacturer's instructions with a total volume of 25ul for each reaction mixture. Total RNA (200 ng) was reverse transcribed at 50ºC during 30 min, followed by 2 min at 94ºC for de-naturation. Complementary DNAs (cDNAs) were then amplified with recombinant Taq-DNA polymerase with 30 cycles of denaturation at 94ºC for 30 s, annealing at 55ºC for 30 s, elongation at 68ºC for 45 s, and followed by a prolonged elongation of 7 min at 68ºC. The primer sequences used for PCR amplification are shown in table 2.1. In order to obtain a semiquantitative assessment of gene expression, data were expressed as normalized ratios by comparing the integrated density values for all genes tested with those for glyceraldehyde- 3-phosphate dehydrogenase (GAPDH). The PCR products were separated by 1% (w/v) agarose gel electrophoresis and visualized by ethidium bromide staining. The images of the gel were captured with a camera and the densitometric analysis of the bands obtained was performed with ImageJ 1.41 software.

Table 2. 1 - Primers for PCR amplification

Gene	Primer sequence (forward)	Primer sequence (reverse)
GAPDH	5'-CAGGACCAGGTTCACCAACAAGT-3'	5'-GTGGCAGTGATGGCATGGACTGT-3'
RUNX-2	5'-CAGTTCCCAAGCATTTCATCC-3'	5'-TCAATATGGTCGCCAAACAG

3.4. Bacterial adhesion

3.4.1. Number of adherent bacteria colonies

A commercial strain of Streptococcus mutans (DSM20523, DSMZ, Germany) was cultivated in sterile tryptic soy broth (TSB, Difco, USA) for 48 h at 37°C. The bacterial solution was harvested by centrifugation at 18°C for 5 min at 2000 rpm and then washed twice and re-suspended in phosphate-buffered saline (PBS, pH7.4, Sigma) solution at a concentration of $1{,}5\times10^8$ colony forming units cells/ml, according to the McFarland standard, using a densitometer (BioMerieux, France). Flat SiO_2 and micropatterned samples of SiO_2, SiO_2 + 1% nanoHA and SiO_2 + 5% nanoHA and a glass control were placed in 24 well-plates with 1 ml of the bacterial suspension

previously prepared, and incubated at 37°C with gentle shaking for 90 min to allow the bacterial adhesion. Three replicates were used for each experiment. After incubation, each sample was gently rinsed twice with PBS to remove non-adherent or loosely adherent bacteria. Then, the samples were transferred into a tube with 5 ml of sterile PBS and sonicated for one second, at 20KHz with a sonicator (Sonopuls HD 2200, Bandelin, Germany) with a MS 73 probe. Finally, serial dilutions of the sonicated solutions were placed onto Brain Heart Infusion (BHI, Liofilchem, Italy) culture plates and after 48 h at 37°C the number of adherent bacteria colonies (Colonies forming Units - CFU) was counted and the number of CFU per mm^2 was calculated.

3.4.2. Morphology

Bacteria morphology was observed using Scanning Electron Microscopy. Bacterial solutions and the incubation were performed as described above. After the 90 minutes of incubation and the washing step to remove non-adherent or barely adherent bacteria, these were fixated with 10% v/v neutral buffered Formalin for 15min. After, the samples were dehydrated as described in 3.1.2.

3.5. Biofilm Formation

A commercial strain of Streptococcus mutans (DSM20523) was cultivated, harvested and incubated along with the various thin films as described in 3.4. After the 90min of incubation, each sample was gently rinsed twice with PBS to remove non-adherent or loosely adherent bacteria. Brain Heart Infusion (BHI, Difco, USA) was added to the culture to provide nutrients for S. mutans proliferation. BHI was changed every day and the culture continued for 72h. Afterwards, biofilm morphology and proliferation were evaluated and the area was quantified by SEM analysis. The samples were fixed and prepared as described in 3.1.2.

4. Statistical analysis

Triplicate experiments were performed. The results were expressed as the arithmetic mean ± standard deviation. The statistical analysis of the results was done using the *one-way analysis of variance* (One-way ANOVA) followed by post hoc Tukey test, with a significance level of $p < 0.05$.

The statistical analysis was performed using the SPSS statistical software (Statistical Package for the Social Sciences Inc., EUA).

III. Results

1. Surface characterization

1.1. *Scanning Electron Microscopy* / Energy Dispersive X-ray Spectroscopy

Scanning electron microscopy results showed that anisotropic silica micropatterned thin films containing different percentages of nanoHA particles were successfully produced. Line-shaped micropatterns faithfully reproduced the mold features with ~5 µm width and height and ~10 µm interspacing, as it may be seen in figure 3.1. EDS analysis of silica samples detected silicon and oxygen, as expected and some components from the glass substrate (Sodium, Potassium) and the SEM coating that consisted of gold and palladium (Figure 3.2 A). The EDS analysis on the nanoHA particles aggregates detected calcium and phosphorus together with elements from the glass substrate (Sodium) and the SEM coating (Gold, palladium). Silicon and oxygen from the silica coating were also detected (Figure 3.2 B).

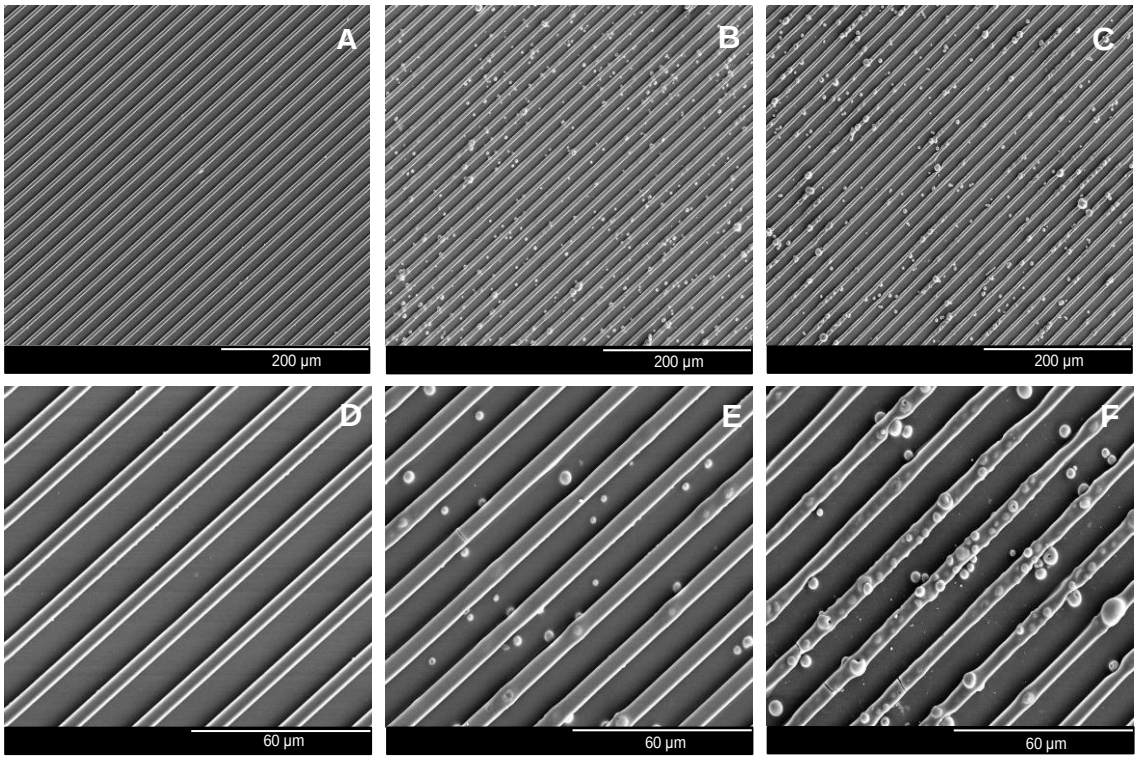

Figure 3. 1 – SEM images of the three types of micropatterned samples produced. (A,D) SiO_2; (B,E) SiO_2 + 1% nanoHA and (C,F) SiO_2 + 5% nanoHA.

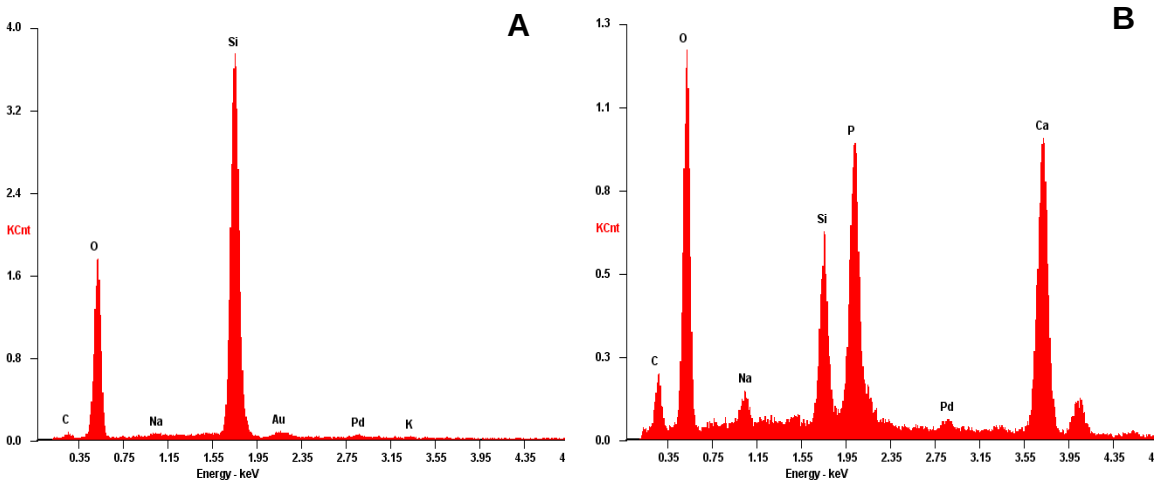

Figure 3. 2 – EDS analysis of Silica sample (A) and a nanoHA particle (B).

1.2. Contact angle

The contact angle measurements were performed with *n=6* and the results are displayed in table 3.1. The flat silica surface presented a hydrophilic behavior. However, with the addition of the patterns, the same silica presented a contact angle with hydrophobic values. With the addition of nanoHA particles, the contact angle also became more hydrophilic.

Table 3. 1 – Contact angle values of the thin films.

Material	Flat SiO_2	Micropatterned SiO_2	SiO_2 + 1% nanoHA	SiO_2 + 5% nanoHA
Θ (º)	38.6 ± 1.6	146.4 ± 3.9	134.6 ± 2.2	121.6 ± 2.2
Image		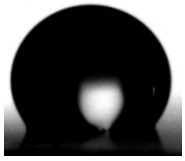	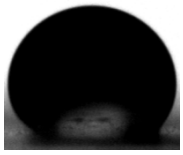	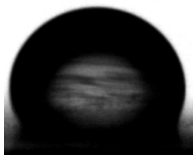

1.3. *X-Ray photoelectron spectroscopy analysis*

The X-Ray photoelectron spectroscopy elemental percentage analysis of the various surfaces is presented in table 3.2. Carbon was detected in all the analyzed surfaces as a usual surface contamination. The silica surface was composed by oxygen and silicon, as expected. As for the two other surfaces, both showed high percentages of oxygen and silicon, however the percentages of calcium and phosphorus were low and very similar in both SiO_2 + 1% nanoHA and SiO_2 + 5% nanoHA.

Table 3. 2 – XPS elemental percentage analysis of the various thin films.

Elements	% Si	% O	% Ca	% P	% C
SiO_2 micropatterned	32.88	59.39	-	-	7.72
SiO_2 + 1% nanoHA	32.66	59.91	0.22	0.19	7.03
SiO_2 + 5% nanoHA	33.09	58.97	0.33	0.16	7.45

2. *In vitro* biological studies

2.1. Basal conditions cell culture

2.1.1. Metabolic Activity

Figure 3.3 shows the results of the Alamar blue assay for cells viability and proliferation. Intra-group analysis showed that there was an increased cell number at all time points in the micropatterned samples. In the TCP control group there was a decrease in the number of cells at day 14. Also, inter-groups analysis showed that MSCs exhibited increased proliferation on the micropatterned 5% nanoHA group with a significant difference ($p<0.05$) when compared to the 1% nanoHA and silica groups at Day 7. Regarding the TCP control group, there was significant higher proliferation of MSCs at day 7, when compared to the other materials.

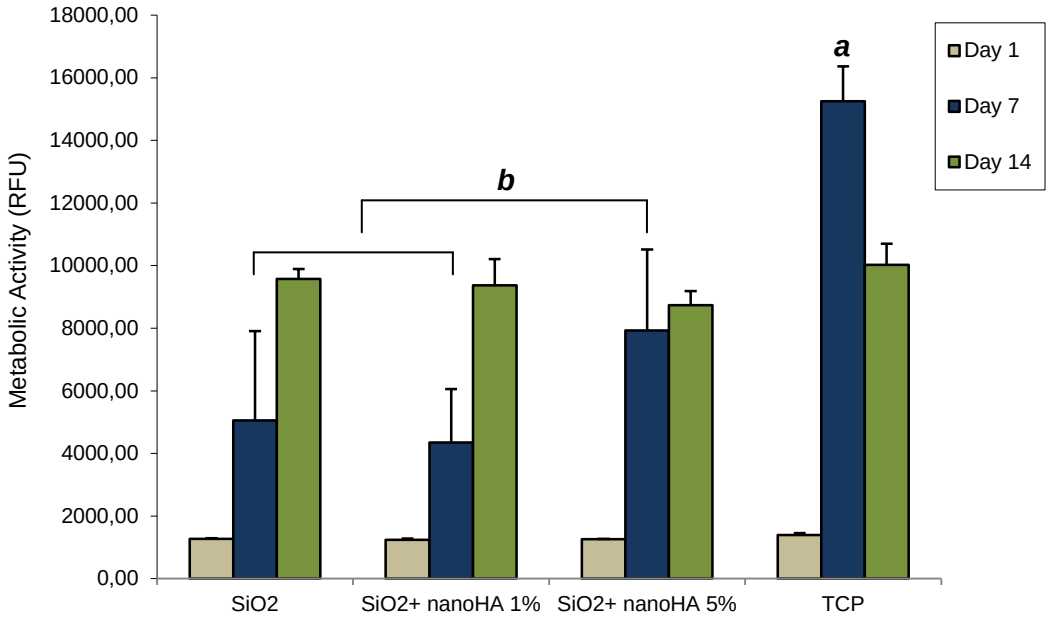

Figure 3. 3 - Mesenchymal Stem cells viability/proliferation at 1, 7 and 14 days using Resazurin. *a, b* represent significant different statistical values at day 7 (*p<0,05*).

2.1.2. Morphology

The observation of the mesenchymal stem cells with fluorescence microcopy showed that cells were well spread and aligned following the texture of micropatterned surfaces starting at Day 1, presenting a much more elongated morphology than the cells cultured on the TCP control group (Figure 3.4). This behavior was more evident for the subsequent time points on all the microtextured surfaces, when compared to the TCPS control group. From day 7 onwards it was already possible to observe that in some areas there is more than one layer of cells all of which were maintaining the same orientation. SEM observations also indicated that cells were well attached, spread and elongated through the thin films surface, while keeping a normal cellular morphology. Cells cytoplasm was extended throughout the micropatterns, with lamellopodia connecting to the patterns and adjacent cells (Figure 3.5). At day 7 of culture, a continuous cell layer was almost formed on all the materials.

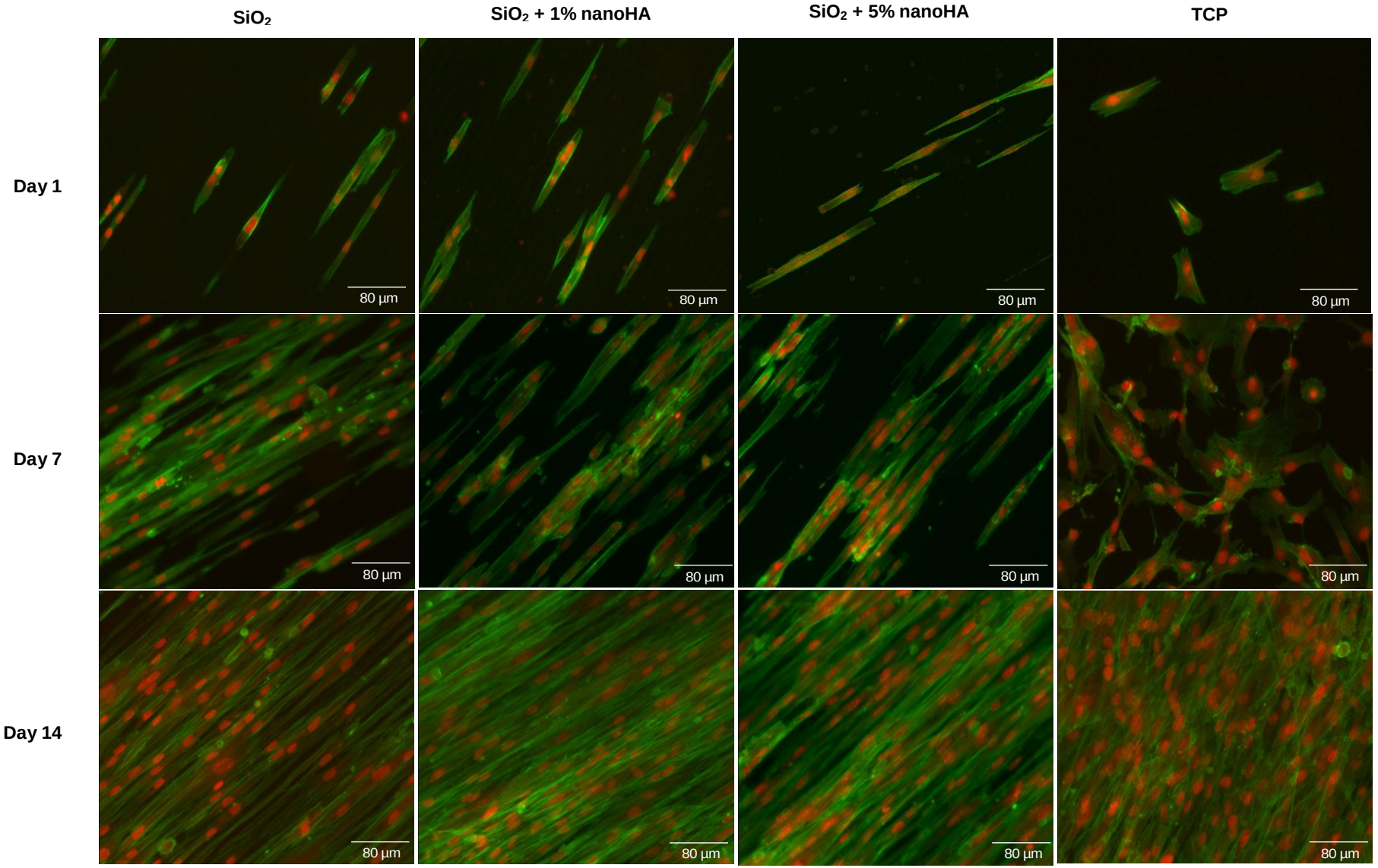

Figure 3. 4 – Cellular morphology on the micropatterned samples and the TCP control at 1, 7 and 14 days of culture.

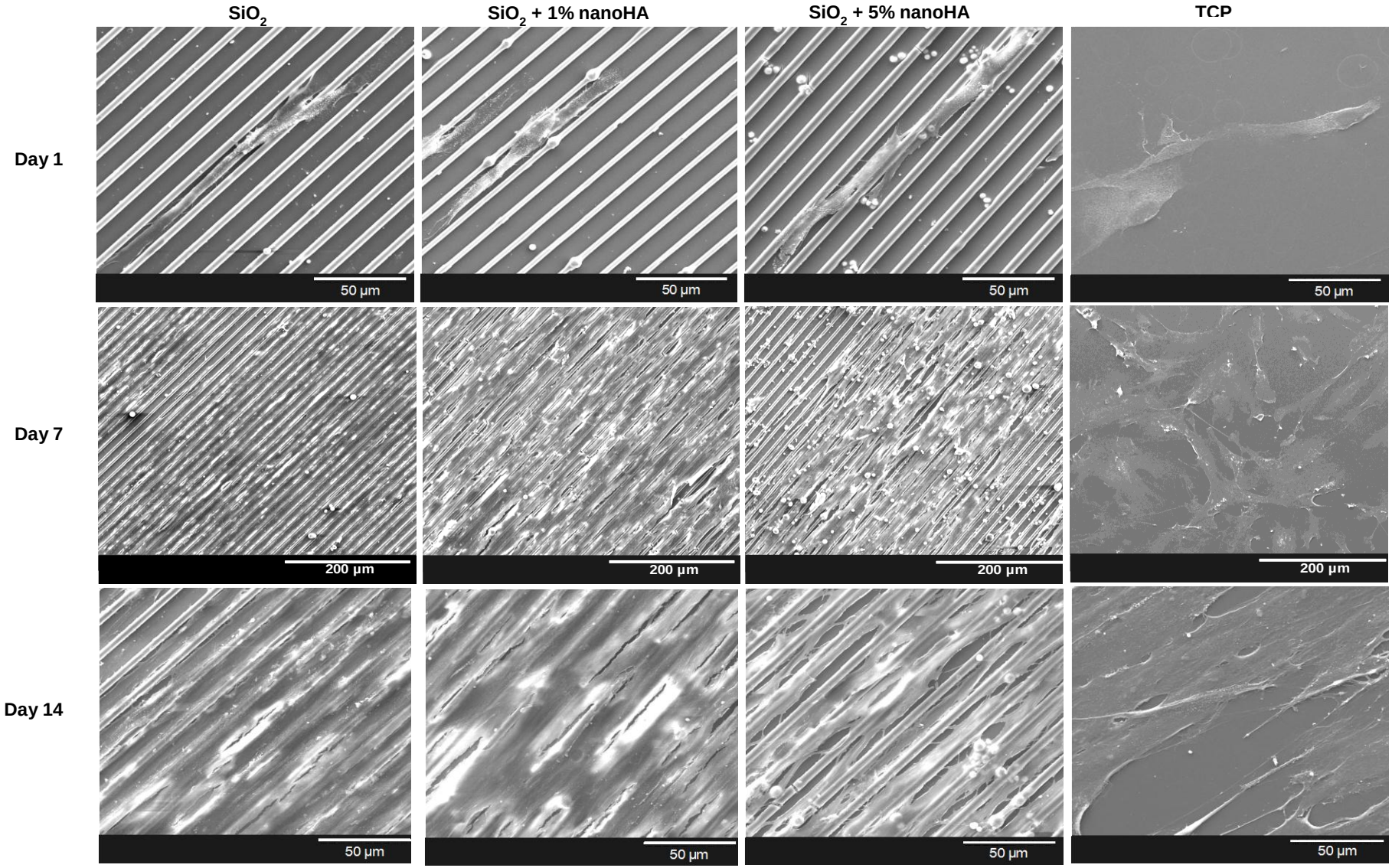

Figure 3. 5 – SEM evaluation of cell morphology on the micropatterned samples and on the TCP control at days 1, 7 and 14 of culture.

2.2. MSCs osteogenic differentiation

2.2.1. Metabolic activity

Figure 3.6 shows the results of cell viability. Cells metabolic activity increased with the time of culture both in the culture with basal conditions and in culture with osteogenic conditions, indicating that cells are metabolically active and proliferating. At day 21, there was a significant increase in the metabolic activity for the culture with osteogenic conditions (*p<0,05*).

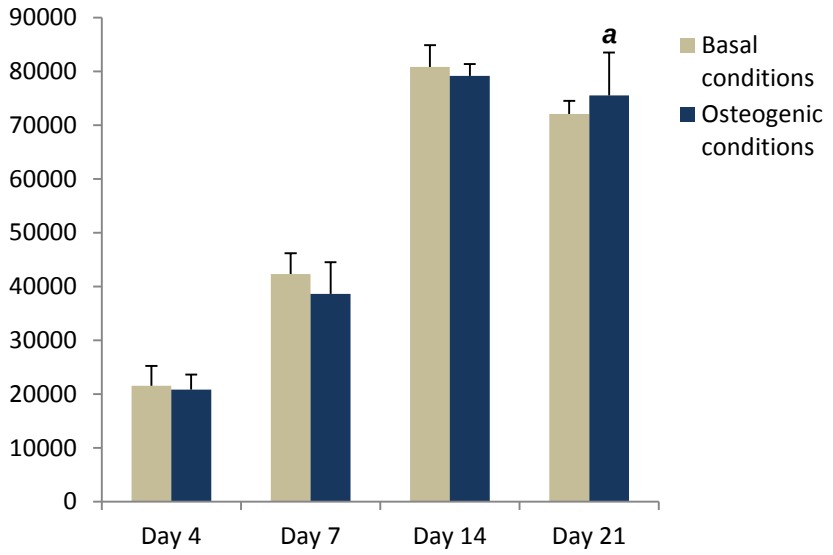

Figure 3. 6 – Metabolic activity of MSC cultured in different conditions at day 4, 7, 14 and 21. *a* represents a significantly different statistical value at day 21 (*p<0,05*).

2.2.2. Alkaline Phosphatase Activity

Regarding the Alkaline Phosphatase activity there was an increase with the time of culture both in the basal conditions culture and in the osteogenic conditions culture. At day 21 the ALP activity in the culture with osteogenic conditions increased significantly when compared to that with basal conditions culture.

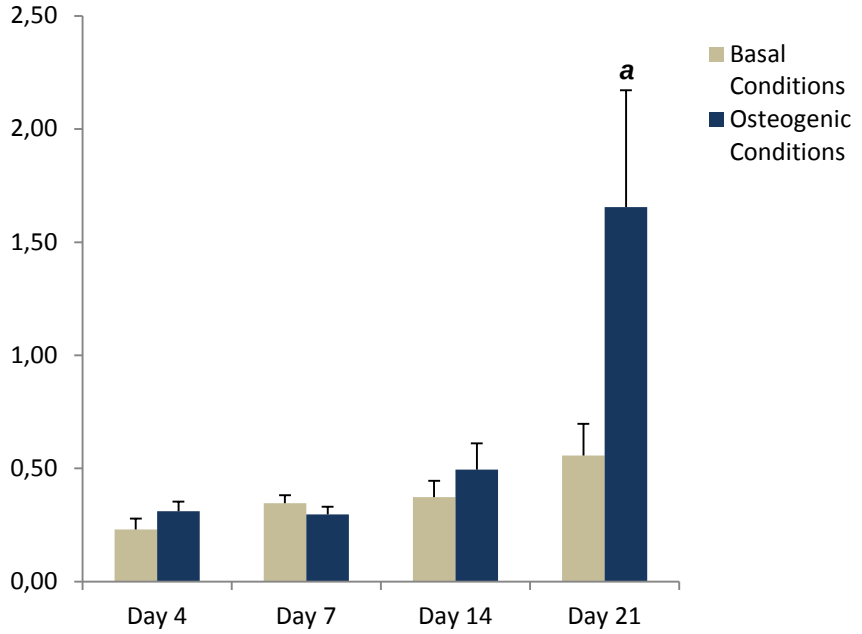

Figure 3. 7 – Alkaline Phosphatase Activity at days 4, 7, 14 and 21. *a* represents a statistically significant difference (*p<0,05*).

2.3. Osteogenic conditions cell culture

2.3.1. Metabolic activity

Again, the resazurin assay was used to determine cell viability and proliferation. Cells metabolic activity on the samples increased at every time point which means that cells proliferated while maintaining their viability during the 21 days of culture. At days 14 and 21, the TCP control had a significant increase in cells proliferation when compared with the other materials (*p<0,05*). Also, in the last time point, SiO_2 + 5% nanoHA group exhibited a significantly increased proliferation when compared to the SiO_2 + 1% nanoHA group.

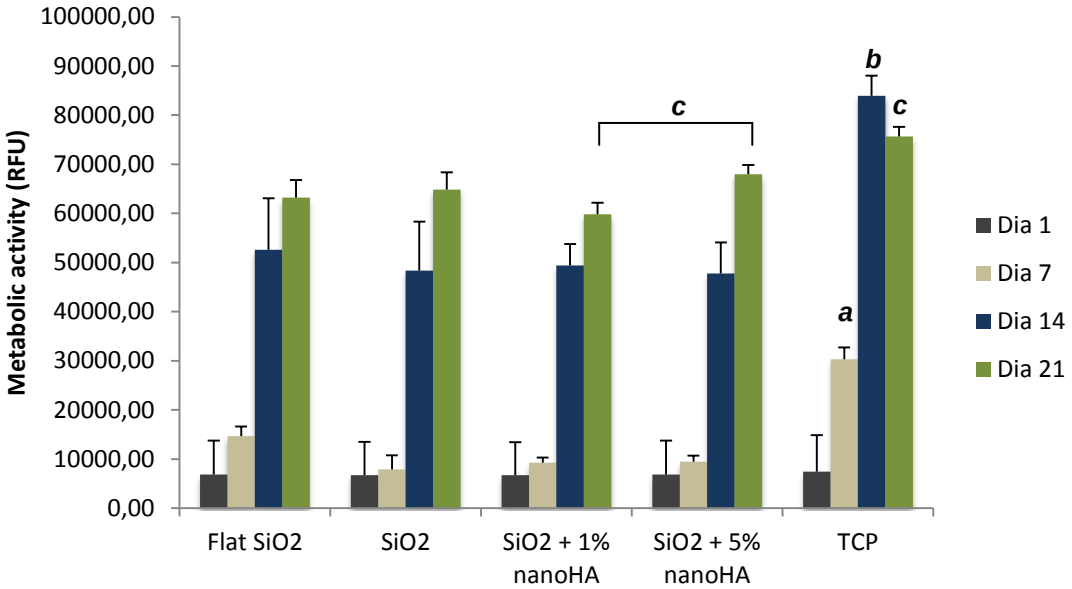

Figure 3. 8 – Metabolic activity in the various materials at all time points of the culture. *a,b* and *c* represent statistically significant differences (*p<0,05*).

2.3.2. Alkaline Phosphatase Activity

Figure 3.9 shows the results of the ALP activity for culture time of 7, 14 and 21 days. ALP increased with culture time in all the materials and the TCP control without statistically significant differences between all the tested surfaces in any time point.

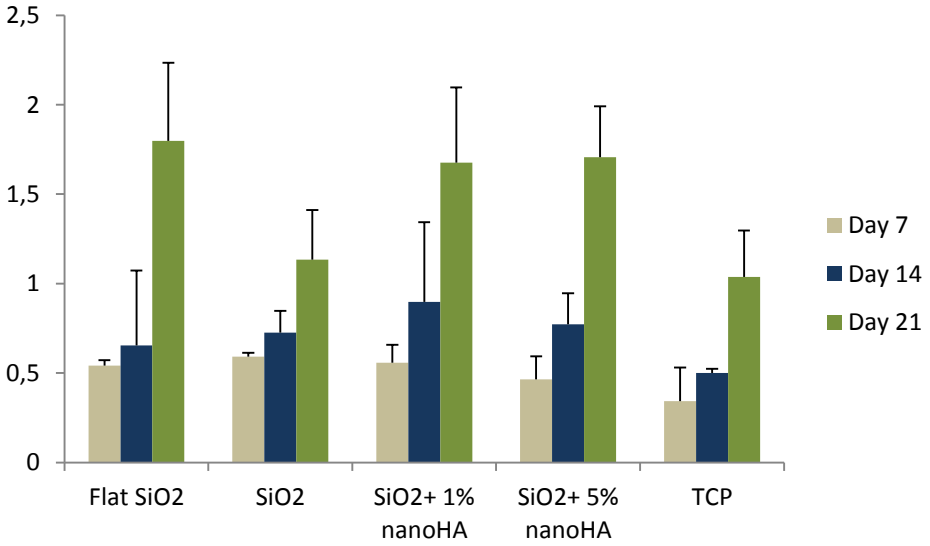

Figure 3. 9 – Alkaline Phosphatase activity at days 7, 14 and 21.

2.3.3. Morphology

With CLSM observation normal cell morphology was identified with the nuclei well distinguished from the cytoplasms. From day 1 cells show an elongated morphology and orientation according to the patterns, which was observed at all time points (Figure 3.10). Cell proliferation along with the time of culture is also observed for all the materials. At days 14 and 21 of culture it was possible to distinguish several layers of cells that still maintained the same specific orientation (Figures 3.12 and 3.13).

SEM evaluation also allowed to identify cells well attached and spread showing a more slimmer and elongated morphology in the micropatterned surfaces. Since day 1 the cells were oriented, following the patterns of the silica surfaces and showing lamellopodia to connect with the material and neighboring cells (Figure 3.14). It was also possible to observe cell-to-cell communication on the top of the patterns at every time point. At day 7 cells were close to each other starting to form a layer of cells (Figure 3.15) and at day 14 the materials surface was completely covered by cells (Figure 3.16). At day 21, SEM observations also allowed to detect that mineralization was occurring in every material except for the TCP control group (Figure 3.17).

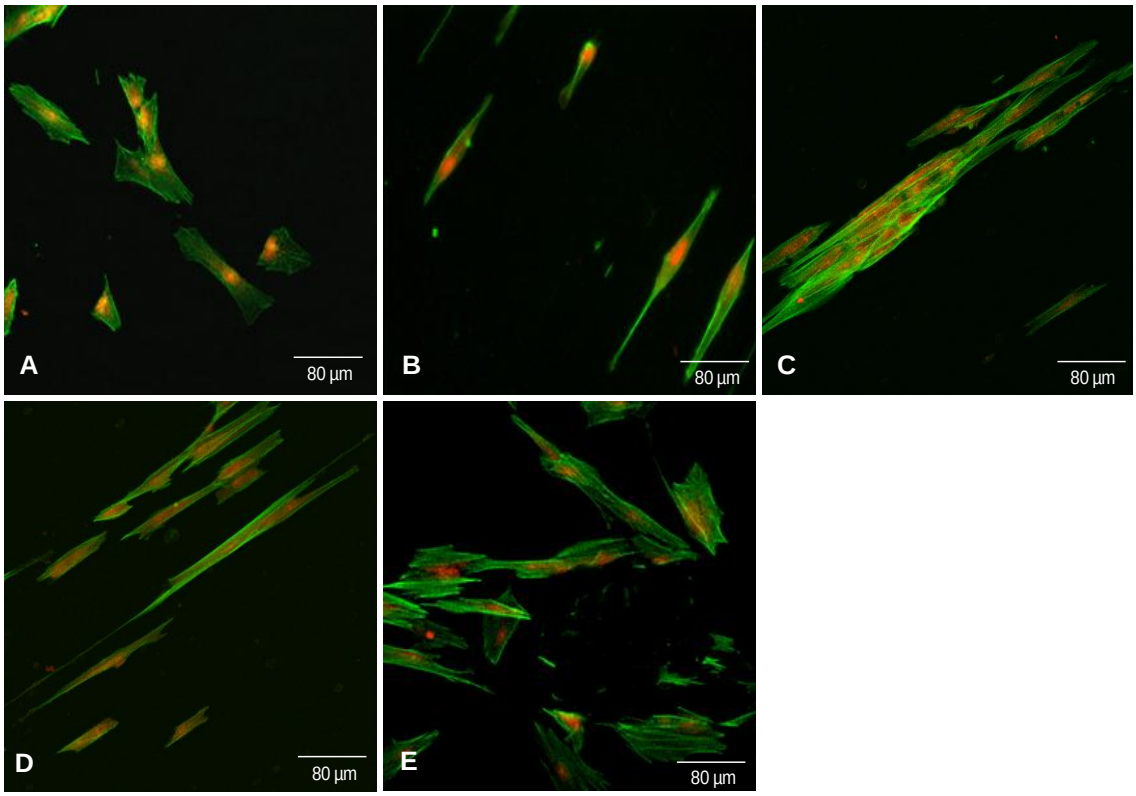

Figure 3. 10 - CLSM observation at day 1 of culture, where: (A) Flat SiO_2; (B) SiO_2; (C) SiO_2 + 1% nanoHA; (D) SiO_2 + 5% nanoHA and (E) TCP. Nuclei were stained with propidium iodide and actin filaments with phalloidin.

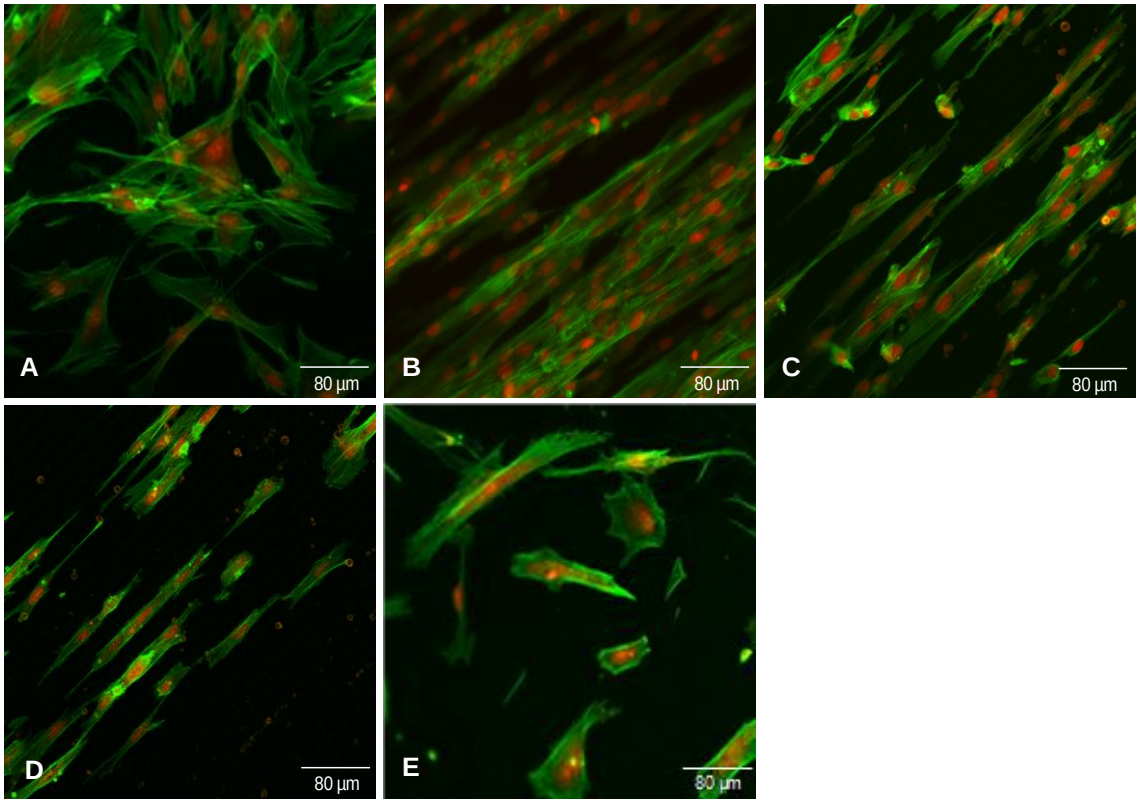

Figure 3. 11 - CLSM observation at day 7 of culture, where: (A) Flat SiO_2; (B) SiO_2; (C) SiO_2 + 1% nanoHA; (D) SiO_2 + 5% nanoHA and (E) TCP. Nuclei were stained with propidium iodide and actin filaments with phalloidin.

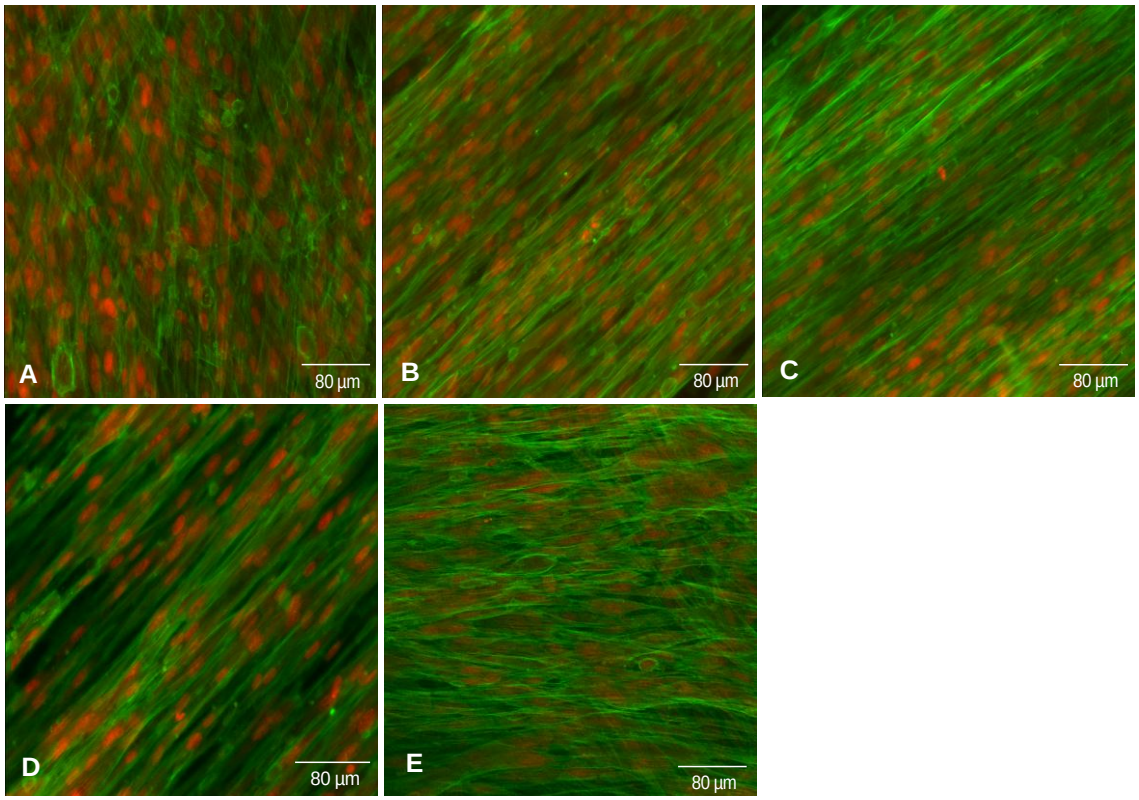

Figure 3. 12 - CLSM observation at day 14 of culture, where: (A) Flat SiO_2; (B) SiO_2; (C) SiO_2 + 1% nanoHA; (D) SiO_2 + 5% nanoHA and (E) TCP. Nuclei were stained with propidium iodide and actin filaments with phalloidin.

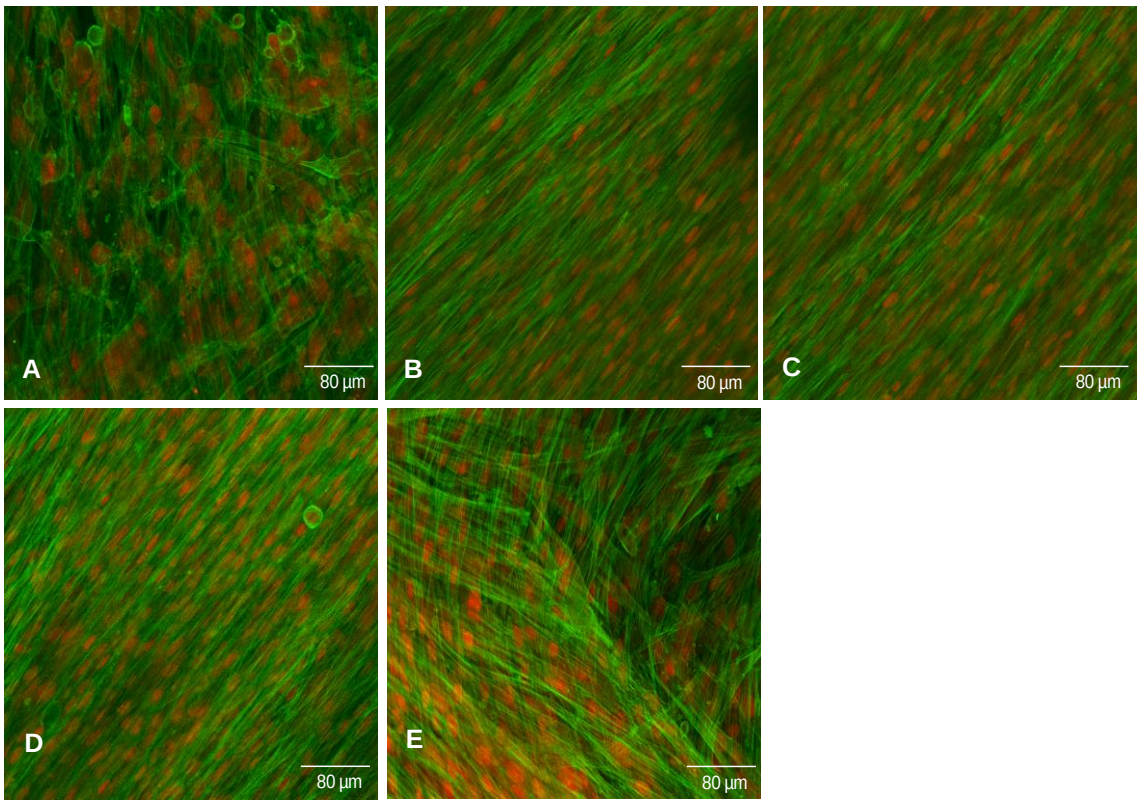

Figure 3. 13 - CLSM observation at day 21 of culture, where: (A) Flat SiO_2; (B) SiO_2; (C) SiO_2 + 1% nanoHA; (D) SiO_2 + 5% nanoHA and (E) TCP. Nuclei were stained with propidium iodide and actin filaments with phalloidin.

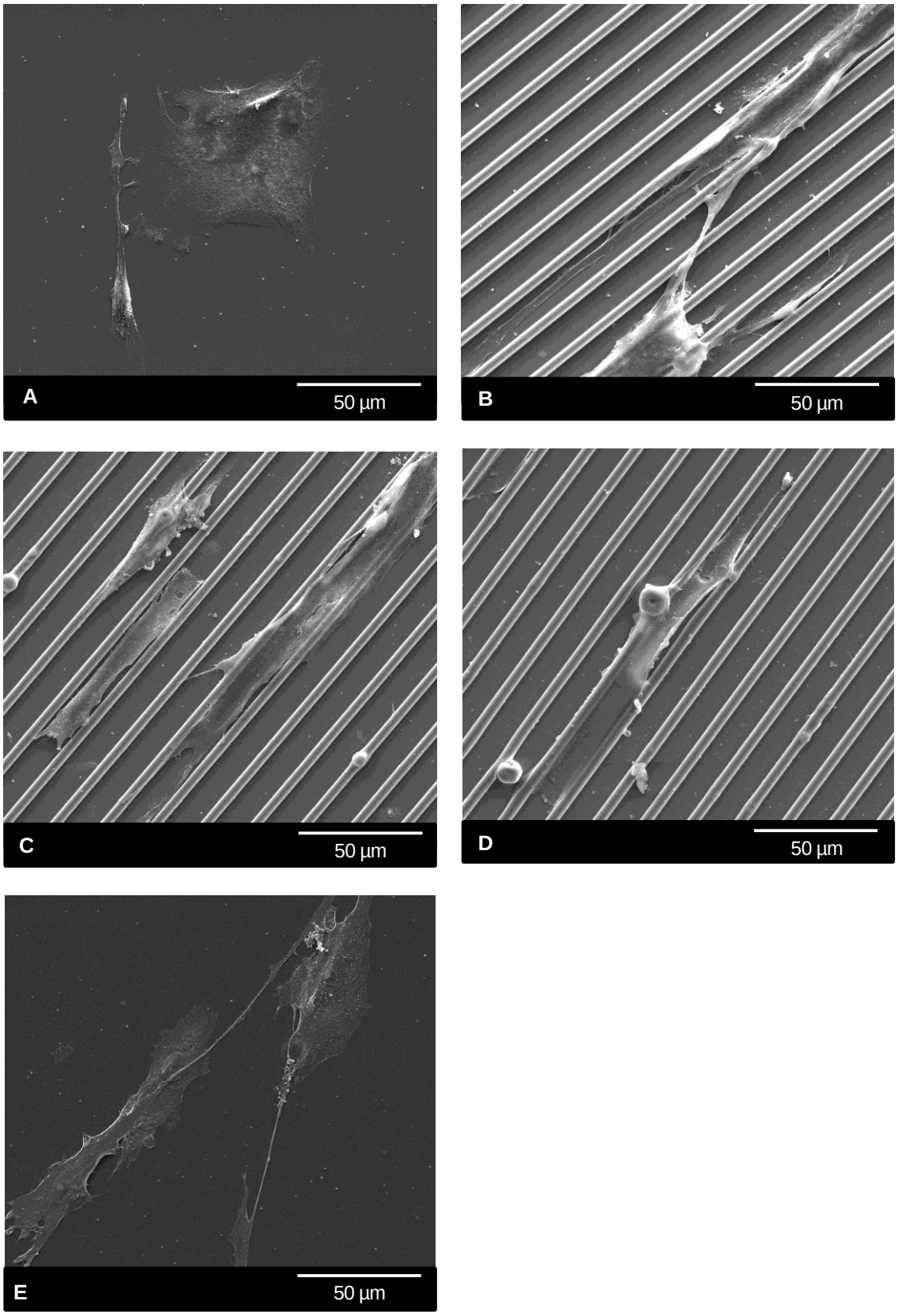

Figure 3. 14 – SEM images at day 1 of culture, where: (A) Flat SiO_2; (B) SiO_2; (C) SiO_2 + 1% nanoHA; (D) SiO_2 + 5% nanoHA and (E) TCP.

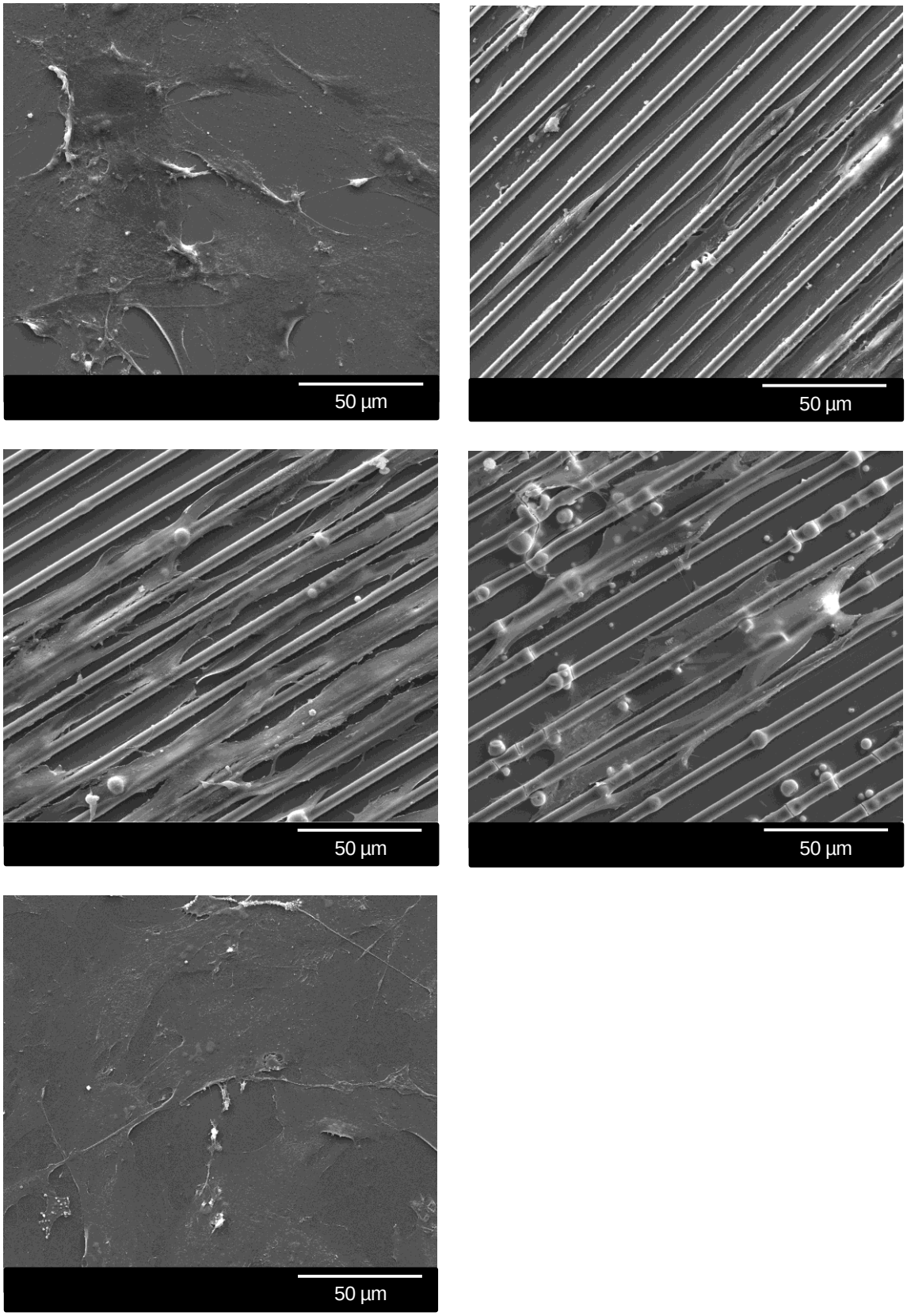

Figure 3. 15 - SEM images at day 7 of culture, where: (A) Flat SiO_2; (B) SiO_2; (C) SiO_2 + 1% nanoHA; (D) SiO_2 + 5% nanoHA and (E) TCP.

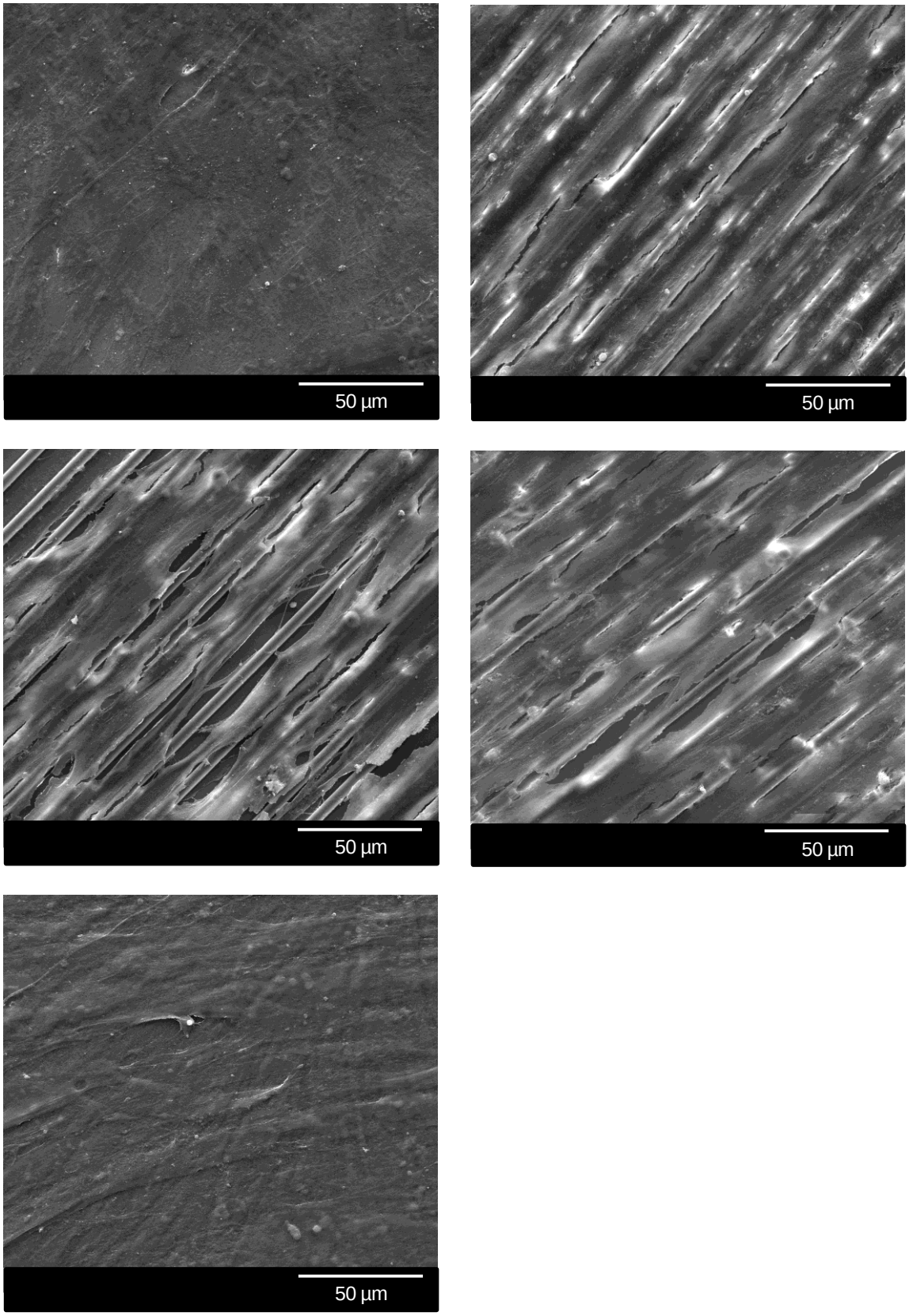

Figure 3. 16 - SEM images at day 14 of culture, where: (A) Flat SiO_2; (B) SiO_2; (C) SiO_2 + 1% nanoHA; (D) SiO_2 + 5% nanoHA and (E) TCP.

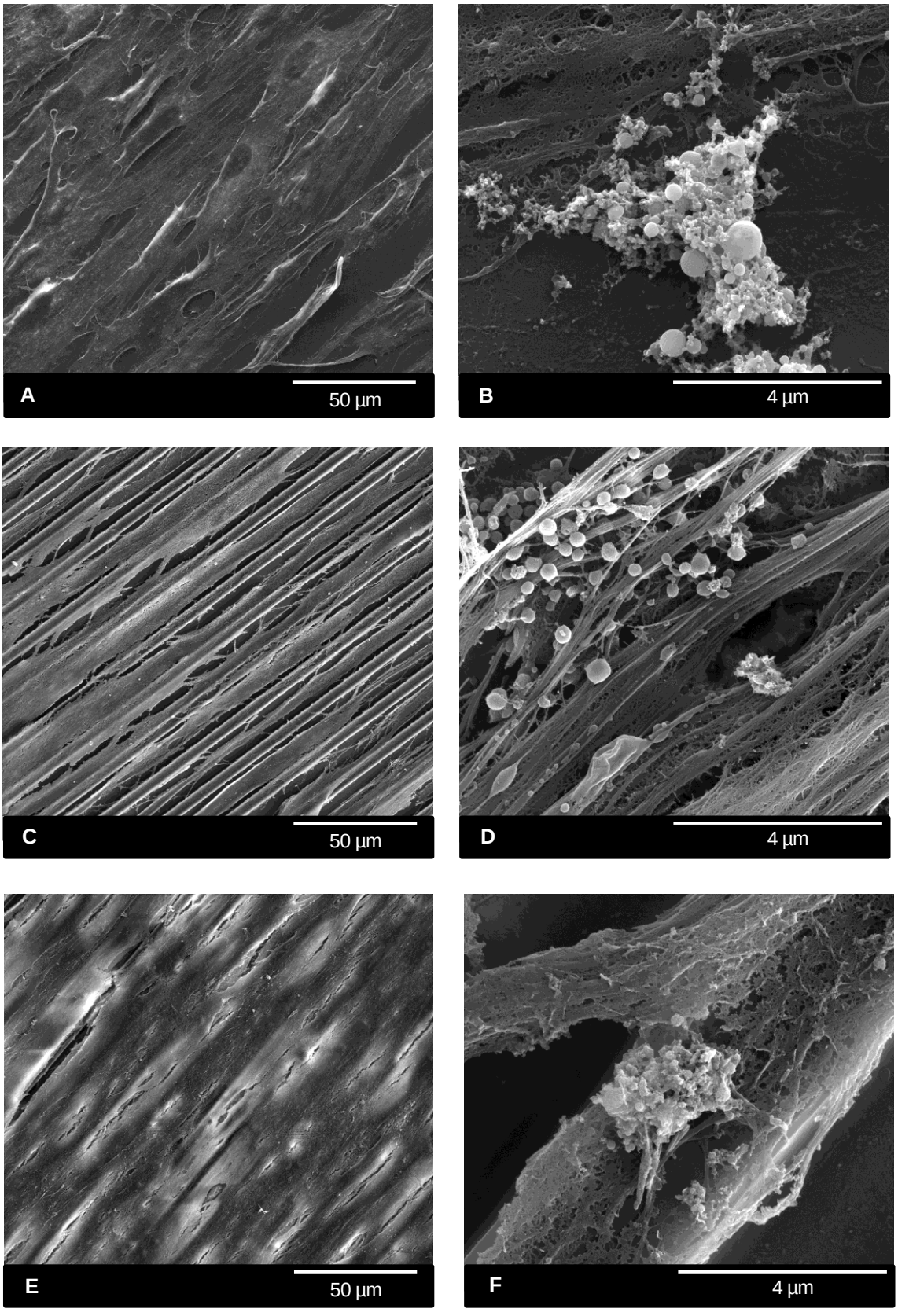
A
50 µm
B
4 µm
C
50 µm
D
4 µm
E
50 µm
F
4 µm

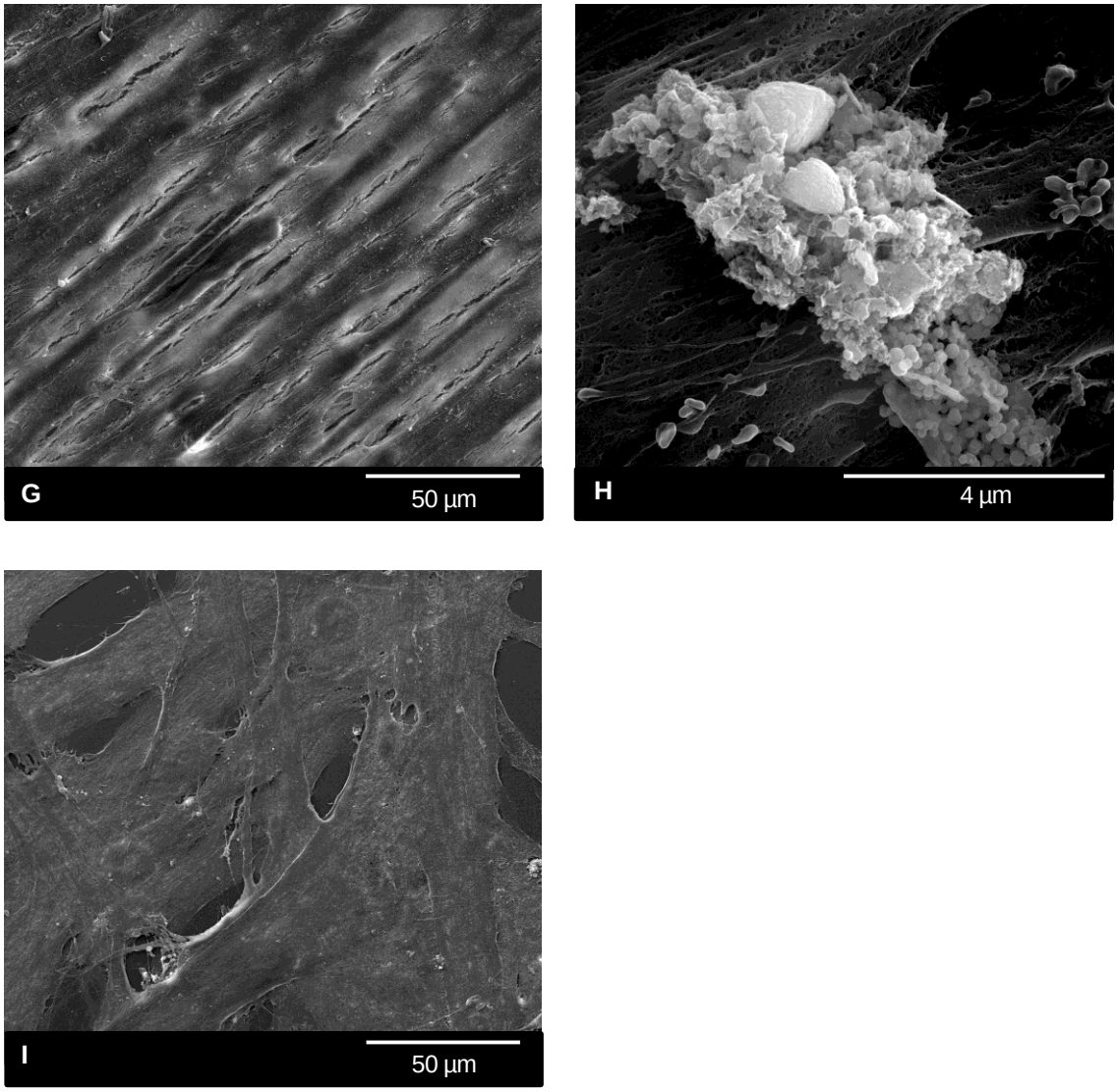

Figure 3. 17 - SEM images at day 21 of culture showing mineralization deposits, where: (A) Flat SiO_2 and (B) respective mineralization; (C) SiO_2 and (D) respective mineralization; (E) SiO_2 + 1% nanoHA and (F) respective mineralization; (G) SiO_2 + 5% nanoHA and (H) respective mineralization and (I)TCP.

2.3.4. Alizarin Red Staining

Alizarin Red Staining detected calcium deposits in all silica thin films. The silica surfaces that contained nanoHA were clearly more stained due to the presence of the particles (it is possible to observe stained nanoHA particles), nevertheless comparing with the stained controls (Figure 3.18 F and G) it is possible to realize that there were more calcium deposits in the materials from the cell culture. In the TCP control group it is difficult to identify calcium deposits although the more stained areas were at the edge of the wells.

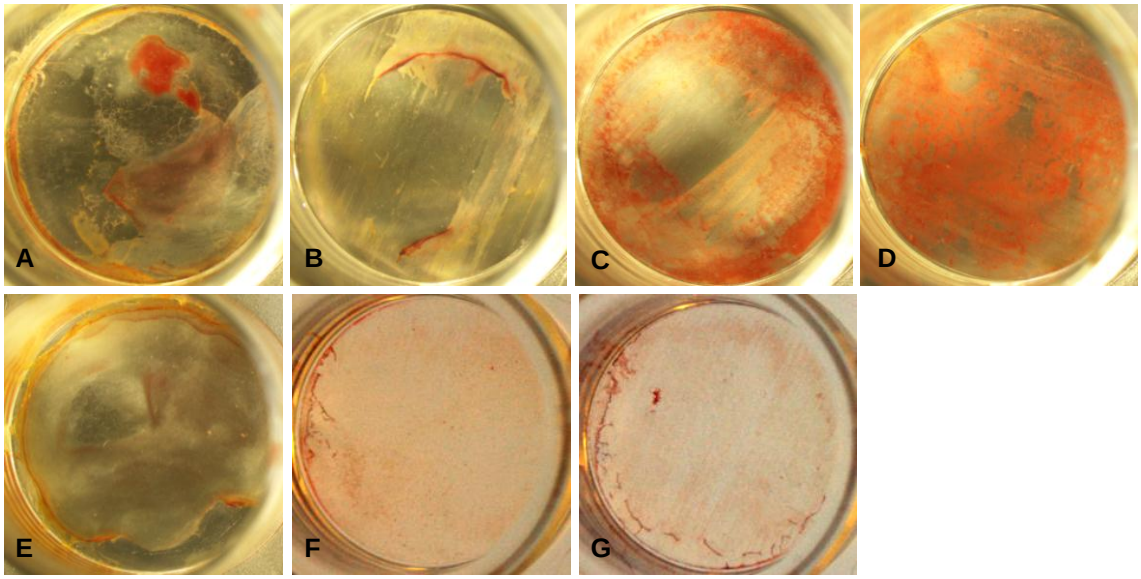

Figure 3. 18 – Alizarin Red Staining shows calcium deposits in orange/red. (A) Flat SiO_2; (B) SiO_2; (C) SiO_2 + 1% nanoHA; (D) SiO_2 + 5% nanoHA; (E) TCP; (F) SiO_2 + 1% nanoHA material control and (G) SiO_2 + 5% nanoHA material control.

2.3.5. Reverse transcriptase polymerase chain reaction (RT-PCR)

The graph below (figure 3.19) shows very preliminary data regarding the Runx2 gene expression. Since, only one measurement could be performed, this graph doesn't show standard-deviation and no statistical analysis was performed. Nevertheless, it is possible to identify a decrease in Runx2 gene expression from day 14 to day 21 in all the patterned materials and the TCP control group. The flat silica surface showed higher expression at day 21.

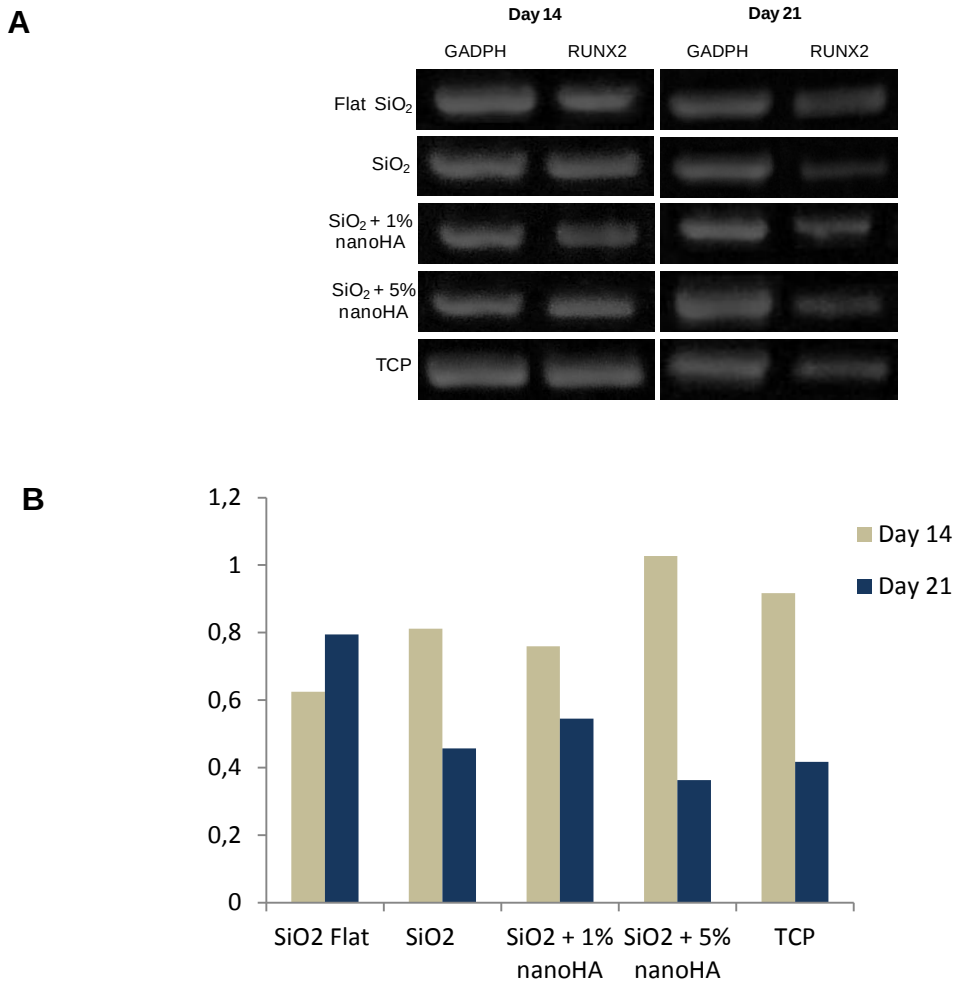

Figure 3. 19 - RT-PCR analysis of RUNX2 for all the materials at days 14 and 21. (A) Representative agarose gel of the PCR results and (B) Densitometric analysis of RUNX2 results, normalized with the corresponding GADPH value.

2.4. Bacterial adhesion

2.4.1. Number of adherent bacteria colonies

The initial *S. mutans* adhesion results are presented in figure 3.20. The flat SiO_2 surface and the glass control were less sustainable surfaces for bacterial adhesion, with significant statistical differences when compared to the other tested materials. Also, the SiO_2 + 5% nanoHA surface had significantly higher *S. mutans* adhesion when compared to the other surfaces ($p<0,05$).

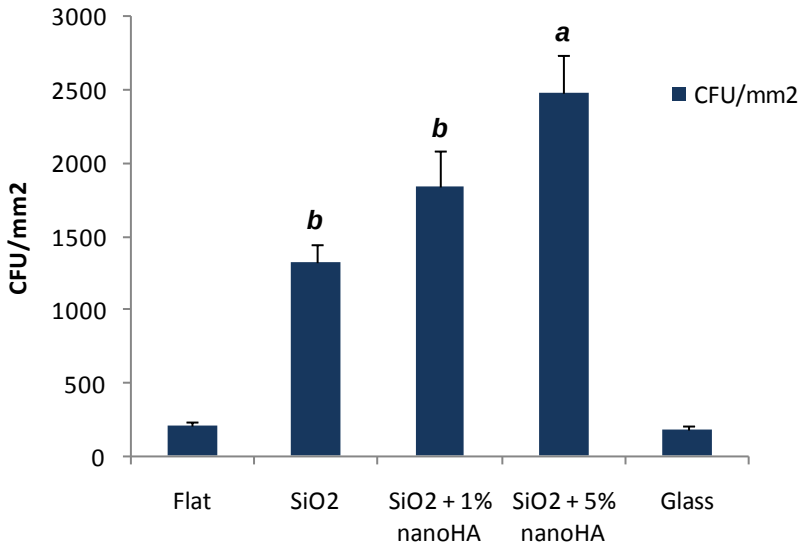

Figure 3.20 – Number of adherent bacteria colonies per mm^2 after 90 minutes of incubation. *a* and *b* represent significantly statistical differences (*p<0,05*).

2.4.2. Morphology

Regarding the bacteria morphology, from SEM results it may be seen that the bacteria present a normal morphology while adherent to the surfaces and it seems that *S.mutans* adhered preferentially at the side of the patterns and also, there are attached bacteria around nanoHA particles (Figure 3.21). At a higher magnification it can be seen that some bacteria aggregates are already starting to create biofilm with production of extracellular polymeric substance (EPS), in figure 3.21 F.

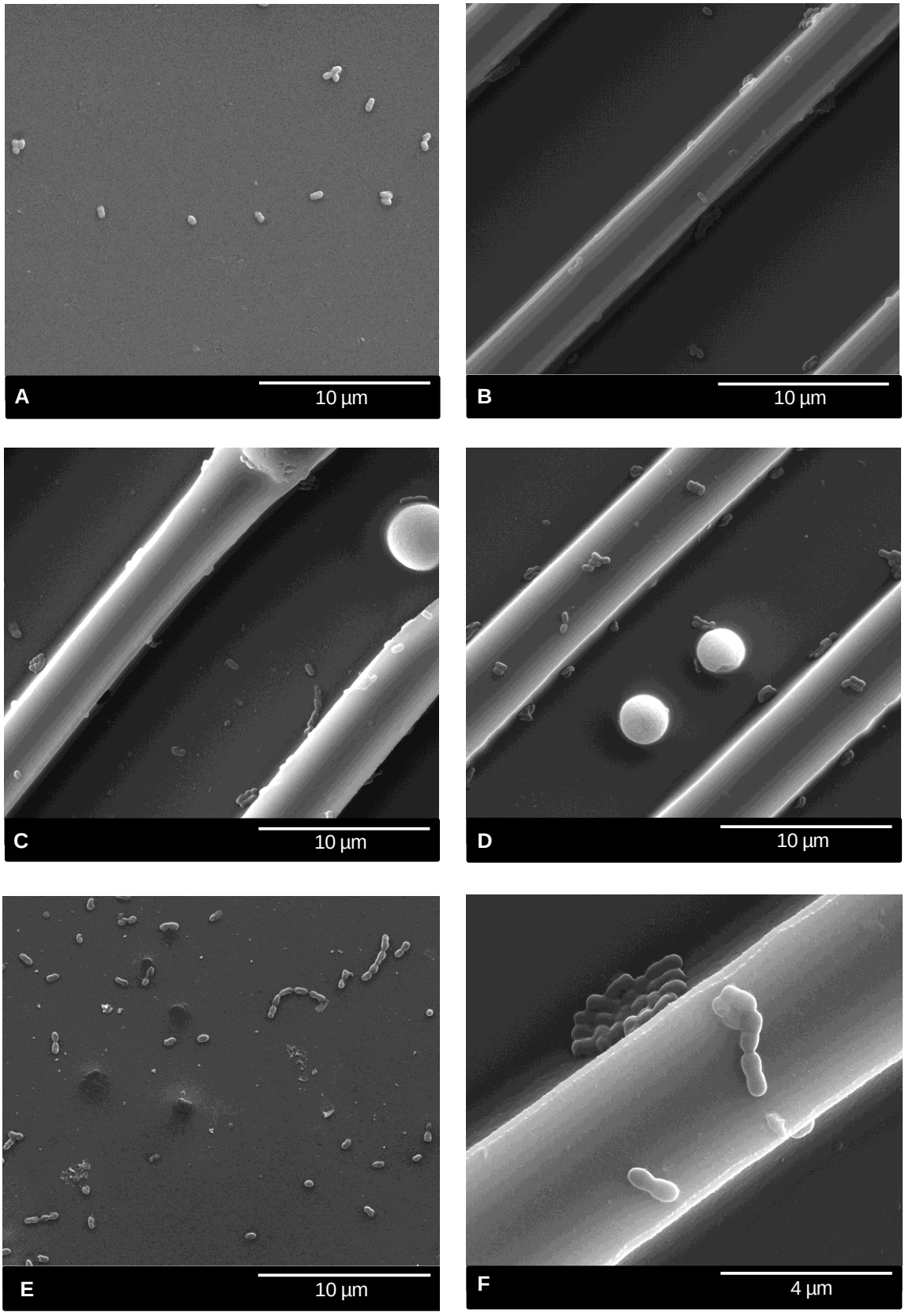

Figure 3. 21 – *S. mutans* morphology and distribution after 90 minutes incubation visualized by SEM. (A) Flat SiO_2; (B) SiO_2; (C) SiO_2 + 1% nanoHA; (D) SiO_2 + 5% nanoHA; (E) Glass control and (F) Biofilm formation on SiO_2.

2.5. Biofilm Formation

A 72h study was carried out in order to evaluate biofilm formation through the calculation of the biofilm area observed by SEM. However, when the surfaces were observed the biofilm had formed heterogeneously on every surface, making it impossible to calculate the biofilm area. In addition, the flat SiO_2 and the glass control surfaces didn't form enough biofilm to allow the calculation of the area (Figures 3.22 - A, B, C and M, N, O). In figure 3.22 it is possible to observe that in the same material, different areas present different amounts of formed biofilm, all with production of extracellular polymeric substances, that play a significant role in mediating the bacterial colonization by providing a matrix for the formation and stabilization of the film architecture.

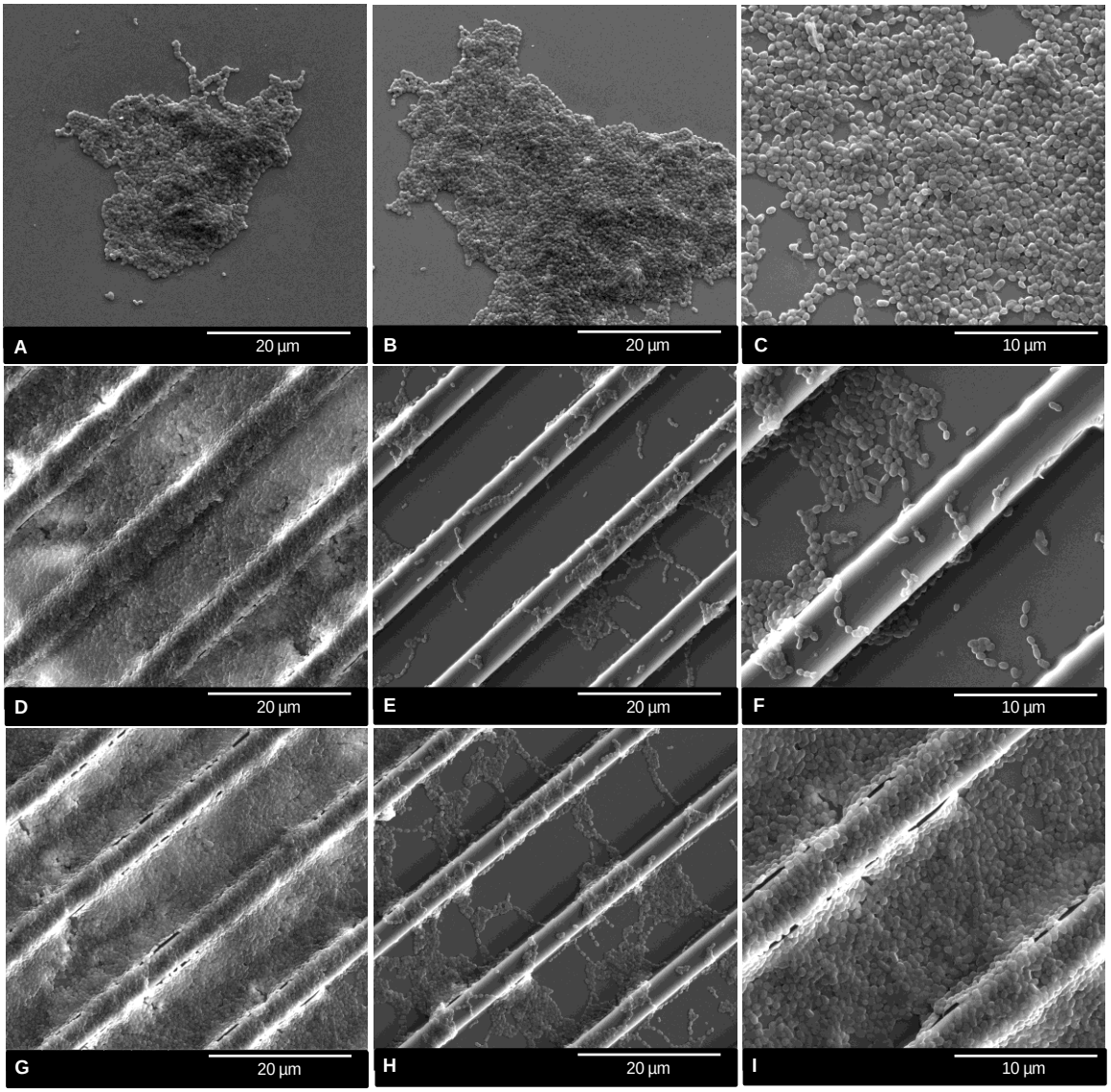

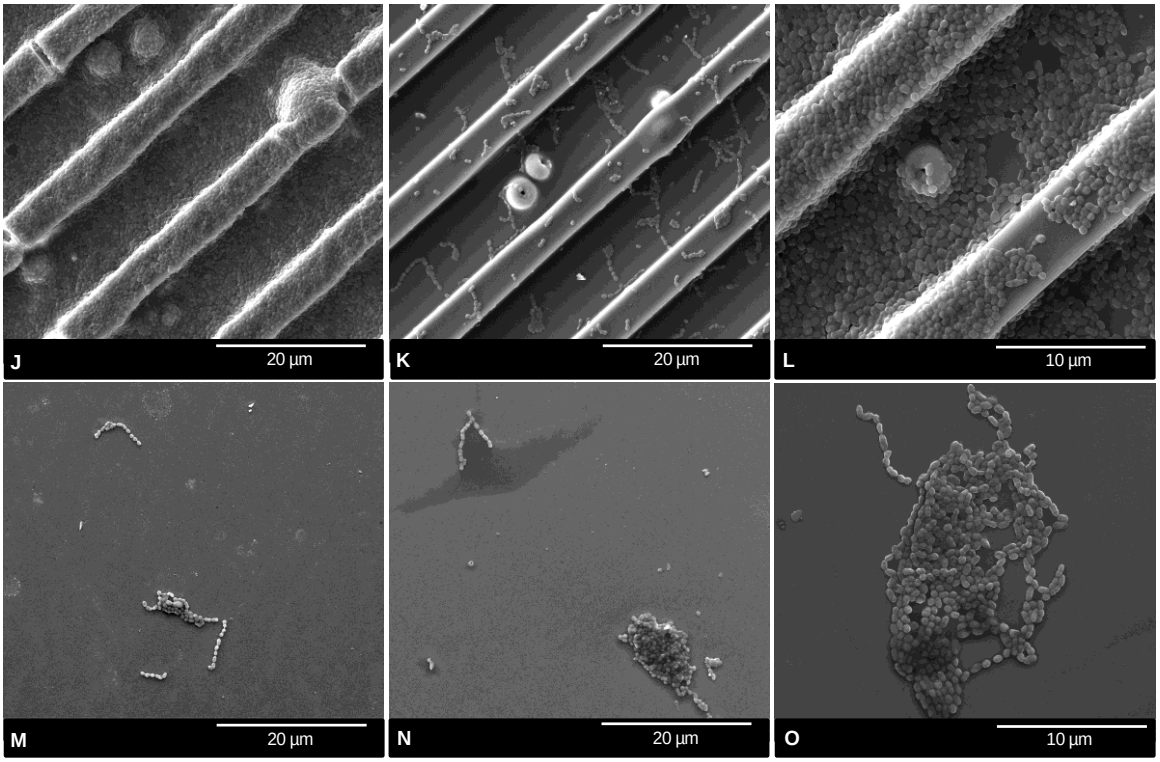

Figure 3. 22 – S.mutans biofilm formation after 72h of incubation. (A, B, C) Flat SiO_2; (D, E, F) SiO_2; (G, H, I) SiO_2 + 1% nanoHA; (J, K, L) SiO_2 + 5% nanoHA and (M, N, O) Glass control.

IV. Discussion

This work proposed a new approach to modify the dental implants surface, using a bioactive and micropatterned silica coating to be applied over zirconia substrates, in order to increase osteointegration and diminish bacterial colonization of dental implants.

Surface characterization showed that different types of micropatterned silica thin films were successfully produced reproducing faithfully the PDMS molds (Figure 3.1).
The hydrophobicity study of the various surfaces showed that contact angle values were being affected by the patterns, a fact that has been described by other authors in the literature [72, 73]. While, the flat silica surface presented a hydrophilic surface, the values obtained for all the patterned materials represented hydrophobic surfaces. Yet, with the addition of nanoHA particles, which are hydrophilic, the contact angle decreased, still within hydrophobic values (Table 3.1) [74].
However, when the samples were positioned with another orientation different contact angle values were obtained. So, in this case, we can assume that the materials are hydrophilic, given the contact angle of the flat silica surface, but the patterns when specifically oriented render the surface hydrophobic.

Regarding the XPS results, low and similar percentages of calcium and phosphorus were detected in both thin films that contained nanoHA particles (Table 3.2). These low and close results in SiO_2 + 1% nanoHA and SiO_2 + 5% nanoHA may be caused by some factors. The first is that the dispersion of the particles is not well controlled and although the materials were evaluated under light microscopy and pre-selected, some materials may have a higher dispersion of nanoparticles in some areas and more accumulation of nanoHA in others. Also, from SEM images (Figure 3.1) it is possible to observe that some nanohydroxyapatite particles are within the silica coating, thus not being detected in the XPS analysis that measures only the top 5nm closer to the surface. These low percentages may also be influenced by this parameter, since the samples are 5µm in height and the analysis is on the order of 5nm, the evaluation is based in surface analysis and therefore is very susceptible to depth and the nanoparticles could be below this analyzed depth. Furthermore, the analysis may be occurring just on the top of the patterns, which leaves a large area without being analyzed.

The in vitro cell cultures showed that all the thin films were citocompatible and capable of maintaining viable cells that proliferate in an oriented fashion at least for 21 days, and were able to differentiate into osteoblasts (Figure 3.7). Cells presented a well spread and more elongated morphology in all the patterned thin films with increasing proliferation at all time points, in both cultures. Also, for the osteogenic condition culture, SEM and Alizarin Red Staining results, at day 21, showed that mineralization was starting to occur in the thin films (Figures 3.17 and 3.18) . In the TCP control group was not possible to detect signs of mineralization during SEM observations, while with alizarin red staining the more stained areas appear at the edge of the well. As just the center bottom of the well was cut to be viewed by SEM, even if there were small signs of mineralization, these would only be seen at the edge of the well.

The nanoHA particles were added to the thin films to increase the bioactivity, the actual contact surface area and osteocondutivity, however this was not observed [28].
Globally, the cell cultures didn't show very significant differences between the various thin films, concerning proliferation (Figures 3.3 and 3.8), ALP activity (Figure 3.9) or the start of the mineralization process (Figure 3.17). Therefore, it might be possible that cells were not recognizing the nanoHA particles, thus suggesting that these could be covered by the silica coatings, as indicated by the XPS results.

Runx2 expression was assessed because this member of the runt family has been identified as a transcription factor critical for osteoblastic differentiation [75, 76]. While it is clearly established that this core binding factor expression is a pre-requisite for osteoblast commitment and differentiation, the dynamic regulation of Runx2 gene expression in mesenchymal stem cells during osteoblast commitment is complex, and involves the integration and convergence of several intracellular signaling pathways and nuclear effectors [76]. The RT-PCR results showed a decrease in Runx2 expression from day 14 to 21, with the exception of the flat silica surface. From these results we can infer that, since Runx2 is a specific transcription factor involved in osteoblast differentiation that is expressed in the beginning of the differentiation process, cells were starting to differentiate at day 14, when the expression is higher and at day 21 a higher number of cells might be already differentiated, thus decreasing the transcription factor expression [76, 77]. Also, since the materials are practically fully covered by several layers of cells, at this point cell proliferation is diminished. Thus, if cells were already differentiating at day 14, there must be a lower number of cells ready for differentiation at day 21 (Figure 3.19).

At this time point, Runx2 expression increased in the flat silica surface, with the possibility that in this material, a higher number of cells are still undergoing differentiation after 21 days.

Concerning bacterial adhesion, all the patterned materials showed significantly higher *S. mutans* adhesion than the flat groups (Flat SiO_2 and glass control). Comparing the number of adherent bacteria in both flat and micropatterned silica it is observed that in the presence of the patterns, the bacterial adhesion increased significantly, since the surface area for contact is much higher [78]. From SEM results it is also possible to observe that *S. mutans* tend to adhere more on the side of the patterns (Figure 3.21). Furthermore, the thin films that contained nanoHA particles showed higher adhesion numbers with SiO2 + 5% nanoHA having a significant higher *S. mutans* adhesion when compared to the rest of the materials (Figure 3.20).
From the previous results concerning surface characterization and cell cultures it seemed very likely that almost all hydroxyapatite nanoparticles are covered by silica. This way, it is not possible to state that the nanoHA particles are increasing the adhesion, but the surface area and roughness that are increased with the introduction of these are. This relationship between surface area, roughness and bacterial adhesion as already been described by several authors [78, 79]

Finally, the biofilm formation results confirmed that *S. mutans* adhered more to the patterned surfaces, since we can see that there is big differences in the amount of biofilm formed between the flat and patterned surfaces (Figure 3.22). Also, EPS production was observed in all the surfaces, an indicator of bacteria virulence making them more resistant to antibiotics [80].

V. Conclusions and Future Work

1. Conclusions

In the present study it was possible to produce different types of micropatterned surfaces with different percentages of nanoHA particles dispersed throughout the surfaces.

From the surface characterization it was observed that the patterns affect the contact angle values and that nanoHA particles weren't totally exposed in the thin films surface, as expected.

In the different cell cultures it was confirmed that the coatings produced are biocompatible and allow cell adhesion and proliferation. The patterned materials affected cell orientation, with these being well spread and with an elongated morphology aligned with the micropatterns. The human pulp derived mesenchymal stem cells were able to differentiate into osteoblast when cultured on the various thin films as it was shown by ALP activity, mineralization signs and Runx2 expression results. Globally, the various coatings didn't present significantly different results in terms of cell behavior, thus confirming what had been indicated by the XPS results, i.e., that the nanoHA particles were barely exposed in the thin films surfaces.

Regarding bacterial adhesion and biofilm formation, all the surfaces allowed bacterial adhesion and proliferation, and EPS production was observed in all the formed biofilms. The patterned surfaces showed significantly higher *S. mutans* adhesion with the SiO_2 + 5% nanoHA surface presenting the highest adhesion values. Therefore, we may conclude that the micropatterned surfaces had increased actual surface area for bacterial adhesion and also that the presence of nanoHA also contributed to increasing the surface area which in turn also increased the bacterial adhesion. The flat silica surface showed the best results between the coatings with the most reduced bacterial adhesion and proliferation.

2. Future Work

Taking into account the results obtained during this work there are some aspects and ideas that can be explored and implemented as future work, that could improve the performance of the desired biomaterial. Such are:

- Adding the nanoHA particles after de-molding, for example by sputtering the nanoHA particles, in order to solve the problem of the particles not being at the top of the silica coating and also trying to better control their dispersion across the silica surfaces.
- To evaluate the thin films degradation and bioactivity in a simulated body fluid (SBF) experiment.
- In addition, in order to make a comparison with the obtained results in this work, this experiment could be used to confirm that there is a silica coating over the nanoHA particles that could be degraded. After the experiment, the materials could be re-evaluated by XPS to check if the elemental percentages of Calcium and Phosphorus have increased. Also, the materials could be ion eroded and be re-evaluated with the same purpose.
- If it is confirmed that the nanoHA particles become more exposed after any of these surface treatments, a cell culture and a bacterial adhesion assays should be repeated in order to confirm the data obtained in the present work.
- A new RT-PCR assay with a wide range of bone associated markers should be repeated for the present cell culture since although Runx2 is specifically linked to osteoblast differentiation it is also possible to find it in other signaling pathways and its single expression does not produce highly significant data.
- Finally, a new model to study biofilm formation should be applied, so as to avoid bacterial deposition over the surfaces placed at the bottom of the wells and instead carry out an active attachment study.

VI. Bibliographic References

[1] Bronzino J.D. *The Biomedical Engineering Handbook, Second Edition*. CRC Press LLC, 2008. ISBN: 084930461X.

[2] Stevens R. *Zirconia and Zirconia Ceramics, Second Edition*. Twickenham: Magnesium Electron, 1986.

[3] Shackelford J.F., et al, *Ceramic and Glass Materials – Structure, Properties and Processing*. Springer, 2008. ISBN: 9780387733616.

[4] Park J. *Bioceramics Properties, Characterization and Applications.* Springer, 2008. ISBN: 9780387095448.

[5] Pinheiro T. *Processamento e caracterização da microestrutura e de algumas propriedades mecânicas da Zircônia parcialmente estabilizada com Ítria e da parcialmente estabilizada com Magnésia.* MD Thesis, Universidade Federal do Rio de Janeiro, Rio de Janeiro, 2008, p.108.

[6] Denry I. and Kelly J.B. State of the art of zirconia for dental applications. *Dental Materials* 24 (2008). p. 299–307.

[7] Gaillard Y., et al, Nanoindentation of Yttria doped Zirconia under Hydrothermal degradation. *Ceramic Engineering and Science Proceedings* 29 (2008) p. 77-92.

[8] Narayan R. *Biomedical Materials*. Springer, 2009. ISBN: 9780387848716.

[9] “Transformation toughening - Encyclopedia Britannica” [Accessed May 29, 2010] Available at: http://www.britannica.com/EBchecked/topic/6681/advanced-structural-ceramics/76760/Transformation-toughening?anchor=ref609427.

[10] Rashad M.M. and Baioumy H.M. Effect of thermal treatment on the crystal structure and morphology of zirconia nanopowders produced by three different routes. *Journal of Materials Processing Technology* 195 (2008) p. 178-185.

[11] WU Y., et al, Processing of alumina and zirconia nanopowders and compacts. *Materials Science and Engineering* A 380 (2004) p. 349-355.

[12] Liu S.Q. *Bioregenerative Engineering Principles and Applications*. John Wiley & Sons, Inc., 2007. ISBN: 9780471709077.

[13] Guleryuz H., et al, Deposition of silica thin films formed by sol–gel method. *Journal of* Sol-Gel *Science and Technology* 54 (2010) p. 249–257.

[14] Podbielska H. and Ulatowska-Jarza A. Sol-gel technology for Biomedical Engineering. *Bulletin of the Polish Academy of Sciences Technical Sciences* 53 (2005) p.261-271.

[15] Arcos D. and Vallet-Regí M. Sol–gel silica-based biomaterials and bone tissue regeneration. *Acta Biomaterialia* 6 (2010) p. 2874–2888.

[16] Pierre A.C. *Introduction to Sol-gel Processing*. Kluwer Academic Publishers, 1998.ISBN: 0792381211

[17] McDonagh C., et al, Characterization of sol-gel-derived silica films. *Journal of Non-Crystalline Solids* 194 (1996) p. 72-77.

[18] Gallardo J. and Galliano P. Thermal Evolution of Hybrid Sol-Gel Silica Coatings: A Structural Analysis. *Journal of Sol-Gel Science and Technology* 19 (2000) p. 393–397.

[19] Iler R.K. The *Chemistry of Silica: Solubility, Polymerization, Colloid and Surface Properties and Biochemistry of Silica.* Wiley-Interscience, 1979. ISBN: 047102404X.

[20] Hench L.L. and Jones J.R. *Biomaterials, artificial organs and tissue engineering.* Woodhead Publishing, 2005. ISBN: 185573737X.

[21] Garcia C. Stability of Suspensions of Bioactive Particles Using Hybrid Organic–Inorganic Solutions as Dispersing Media. *Journal of Sol-Gel Science and Technology* 34 (2005) p.211–217.

[22] Klein L.C. *Sol-Gel Technology for Thin Films, Fibers, Preforms, Electronics, and Specialty Shapes.* Noyes Publications, 1998. ISBN: 081551154X.

[23] “Sol-Gel Coatings” [Accessed June 8, 2010]. Available at: http://commons.wikimedia.org/wiki/File:SolGel_SpinCoating.jpg.

[24] Catauro M., et al, Sol–gel processing of anti-inflammatory entrapment in silica, release kinetics, and bioactivity. *Journal* of *Biomedical* Materials Research 87 (2008) p. 843-849.

[25] López A.J., et al, Laser densification of sol–gel silica coatings on aluminium matrix composites for corrosion and hardness improvement. *Surface & Coatings Technology* 203 (2009) p.1474-148

[26] Hench L.L. Sol-gel materials for bioceramic Applications. *Solid State & Materials Science* 2 (1997) p. 604-610.

[27] Hamadouche M., et al, Long term in vivo bioactivity and biodegradability of bulk sol–gel bioactive glasses. *Journal* of *Biomedical* Materials Research 54 (2001) p.560-566.

[28] Ferraz M.P., et al, Hydroxyapatite nanoparticles: A review of preparation methodologies. *Journal of Applied Biomaterials & Biomechanics* 2 (2004) p. 74-80.

[29] Wahl D.A. and Czernuszka J.T. Collagen-Hydroxyapatite Composites for Hard Tissue Repair. *European Cells and Materials* 11 (2006) p. 43-56.

[30] Webster TJ, et al, Enhanced surface and mechanical properties of nano phase ceramics to achieve Orthopedic/dental implant efficacy. *Key Engineering Materials* 192; 5 (2001) p. 321-324.

[31] Manuel C.M., et al, Synthesis of hydroxyapatite and tricalcium phosphate nanoparticles - preliminary studies. *Key Engineering Materials* 240-242 (2003) p. 555-8.

[32] Ito Y. Surface micropatterning to regulate cell functions. *Biomaterials* 20 (1999) p. 2333-2342.

[33] Mendonça G., et al, Advancing dental implant surface technology – from micron to Nanotopography. *Biomaterials* 29 (2008) p. 3822–3835.

[34] Lam M., et al, Reversible on-demand cell alignment using reconfigurable microtopography. *Biomaterials* 29 (2008) p. 1705-1712.

[35] Xia Y. and Whitesides G.M. Soft-Lithography. *Annual Review of Materials Research* 28 (1998) p. 153–84.

[36] Sakka, Sumio. *Handbook of Sol–Gel Science and Technology Processing, Characterization and Applications.* Vol II. Kluwer Academic Publishers. ISBN: 1402079672.

[37] "Nanoterra – Soft-lithography" [Accessed July 2, 2011]. Available at: http://www.nanoterra.com/soft_lithography.asp.

[38] Weibel D.B., et al, Microfabrication meets microbiology. *Nature Reviews Microbiology* 5 (2007) p. 209–218

[39] Gutwein LG and Webster TJ. Increased viable osteoblast density in the presence of nanophase compared to conventional alumina and titania particles. *Biomaterials* 25 (2004); p. 4175–4183.

[40] Price RL., et al. Osteoblast function on nanophase alumina materials: influence of chemistry, phase, and topography. Journal of Biomedical Materials Research A 67 (2003) p. 1284–1293.

[41] Schwartz Z., et al. Surface microtopography regulates osteointegration: the role of implant surface microtopography in osteointegration. Alpha Omegan 98 (2005) p. 9-19.

[42] Pelaez-Vargas A., et al, Cells spreading on Micro-fabricated Silica Thin film Coatings. *Microscopy* and *Microanalysis* 15 (supp 3), 2009.

[43] Craighead H.G., et al, Chemical and topographical patterning for directed cell attachment. *Current Opinion in Solid State and Materials Science* 5 (2001), p.177-184.

[44] Meshorer E and Plath K. *The Cell Biology of Stem Cells - Advances in Experimental Medicine and Biology*. Vol. 695. Springer Science+Business Media, LLC, 2010. ISBN: 978-1-4419-7036-7.

[45] Bajada, S., et al, *Chapter 13: Stem Cells in Regenerative Medicine*, in Topics in Tissue Engineering, Vol.4. E-Book. Expertissues, 2008.

[46] Deng H. and Liu Y. *Current Topics in Bone Biology*. World Scientific, 2005. ISBN: 981-256-209-5.

[47] Bilezikian J.P., et al, *Principles of Bone Biology, 3rd Edition*. Academic Press, 2008. ISBN: 978-0120986507.

[48] Vemuri M.C., et al, *Mesenchymal Stem Cell Assays and Applications*. Humana Press, 2011. ISBN 978-1-60761-998-7.

[49] D'aquino R., et al, Human Dental Pulp Stem Cells: From Biology to Clinical Applications. *Journal of Experimental Zoology* B: *Molecular and Developmental Evolution* (2008) 310b.

[50] Mauth C., et al, *Chapter 3 - Restorative Applications for Dental Pulp Therapy*, in Topics in Tissue Engineering. Vol.3. E-Book. Expertissues, 2007.

[51] D'Aquino R., et al, Dental Pulp Stem Cells: A Promising Tool for Bone Regeneration. *Stem Cell Rev* 4 (2008) p. 21–26.

[52] Graziano A., et al, Scaffold's Surface Geometry Significantly Affects Human Stem Cell Bone Tissue Engineering. Journal of *Cellular Physiology* 214 (2008) p.166–172.

[53] "Dental Stem Cells" [Accessed on June 29, 2011]. Available at: http://rxdentalspa.com/?page=dental_stem_cell.

[54] Meyer U., et al, *Fundamentals of Tissue Engineering and Regenerative Medicine.* Springer, 2009. ISBN: 9783540777540.

[55] Lieberman J.R. and Friedlaender G.E. *Bone Regeneration and Repair Biology and Clinical Applications*. Humana Press, 2005. ISBN: 0896038475.

[56] Meyer U. and Wiesmann H.P. *Bone and Cartilage Engineering*. Springer, 2006. ISBN: 3540253475.

[57] Stevens M.M. Biomaterials for bone tissue engineering. *Materials Today* 11; 5 (2008) p. 18-25.

[58] "Bone Remodeling – University of Michigan" [Accessed July 4, 2010]. Available at: http://www.ns.umich.edu/Releases/2005/Feb05/bone.html.

[59] Harris LG, et al, Staphylococcus aureus adhesion to titanium oxide surfaces coated with non-functionalized and peptide functionalized poly(l-lysine)-grafted-poly(ethylene glycol) copolymers. *Biomaterials* 25 (2004). p.4135 –4148.

[60] Vassiliki A., et al, *Staphylococcus aureus* adhesion to self-assembled monolayers: effect of surface chemistry and fibrinogen presence. *Colloids and Surfaces B: Biointerfaces* 24 (2002). p. 217–228.

[61] Pye A.D., et al, A review of dental implants and infection. *Journal of Hospital Infection* 72 (2009) p.104-110.

[62] Shemesh M., et al, Genetic adaptation of Streptococcus mutans during biofilm formation on different types of surfaces. *BMC Microbiology* 10 (2010) p. 1-10.

[63] Galanakos S.P., et al, Biofilm and orthopaedic practice: the world of microbes in a world of implants. *Orthopaedics and Trauma* 23 (2009) p. 175-179.

[64] Scarano A., et al, Bacterial Adhesion on Commercial Pure Titanium and Zirconium Oxide Disks: An In Vivo Human Study. *Journal of Peridontology* 75 (2004) p. 292-296.

[65] Leonhardt A., et al, Microbial findings at failing implants. *Clinical Oral Implants Research* 10 (1999) p. 339-345.

[66] Rocha S., et al, *Streptococcus mutans* Attachment on a Cast Titanium Surface. *Materials Research* 12 (2009) p.41-44.

[67] Hajishengallis G., *Porphyromonas gingivalis* e host interactions: open war or intelligent guerilla tactics? *Microbes and Infection* 11 (2009) p. 637-645.

[68] Nociti FH Jr, et al, Clinical and microbiological evaluation of ligature-induced peri-implantitis and periodontitis in dogs. *Clinical Oral Implants Research* 12; 4 (2001) p. 295-300.

[69] "Perio.org" [Accessed July 12, 2010] Available at: http://www.perio.org/consumer/2a.html.

[70] Shelburne, C.E., et al., Differential display analysis of Porphyromonas gingivalis gene activation response to heat and oxidative stress. *Oral Microbiology and Immunology* 20 (2005) p.233-238.

[71] Grey W.T., et al, Expression of the Streptococcus mutans fructosyltransferase gene within a mammalian host. *Infection and Immunity* 65 (1997) p. 2488–2490.

[72] Pacifico J., et al, Superhydrophobic Effects of Self-Assembled Monolayers on Micropatterned Surfaces: 3-D Arrays Mimicking the Lotus Leaf. *Langmuir* 22 (2006) p. 11072-11076.

[73] Tadanaga K., et al, Micropatterning of SnO_2 thin films using hydrophobic–hydrophilic patterned surface. *Ceramics International* 30; 7 (2004) p.1815-1817.

[74] Ribeiro N., et al, Influence of crystallite size of nanophased hydroxyapatite on fibronectin and osteonectin adsorption and on MC3T3-E1 osteoblast adhesion and morphology. *Journal of Colloid and Interface Science* 351 (2010) p. 398-406.

[75] Yang S., et al, In Vitro and In Vivo Synergistic Interactions between the Runx2/Cbfa1 Transcription Factor and Bone Morphogenetic Protein-2 in Stimulating Osteoblast Differentiation. *Journal of Bone and Mineral Research* 18; 4 (2003) p. 705-715.

[76] Tou L., et al, Transcriptional regulation of the human Runx2/Cbfa1 gene promoter by bone morphogenetic protein-7. *Molecular and Cellular Endocrinology* 205 (2003) p. 121-129.

[77] Ducy P., et al, Osf2/Cbfa1: A Transcriptional Activator of Osteoblast Differentiation. *Cell* 89; 5 (1997) p. 747-754.

[78] Katsikogianni M. and Missirlis Y.F. Concise Review of Mechanisms of Bacterial Adhesion to Biomaterials and of Techniques Used in Estimating Bacteria-material Interactions. *European Cells and Materials* 8 (2004) p. 37-57.

[79] Mei L., et al, Influence of surface roughness on streptococcal adhesion forces to composite resins. *Dental Materials* 27; 8 (2011) p. 770-778.

[80] Vu B., et al, Bacterial Extracellular Polysaccharides Involved in Biofilm Formation. *Molecules 14 (*2009) p. 2535-2554